1 Crystallographic and Microstructural Considerations

The bulk properties of a solid, such as conductivity, magnetism, and second harmonic generation, hinge on the solid's structure, which, in turn, is normally that arrangement of a material's fundamental particles (molecules, atoms, or ions), with the lowest potential energy as a function of all the atomic positions. We have learned through computational approaches that interatomic potential energy is a function of short-range, long-range, and many-body interactions. For molecular-based substances, one must also consider van der Waals interactions, hydrogen bonds, and capillary and hydrophobic forces. At first glance, these noncovalent forces may seem of secondary importance, but their influence on governing the particular structure adopted by a substance, and hence its resulting properties, can be striking. Organic chemists have long been aware of this. For example, the double-helical structure of DNA is, to a large degree, a consequence of hydrogen bonding between the base pairs. In recent years, supramolecular chemists have focused attention on noncovalent structure-directing intramolecular and intermolecular interactions in the spontaneous formation of ordered aggregates, appropriately termed *chemical self-assembly processes*. It has been applied increasingly to the synthesis of hybrid organic–inorganic materials. However, due to certain limitations, self-assembly of purely inorganic substances, particularly materials in the micro- to millimeter size range (Section 1.5.2), is still in its infancy.

Externally, crystals typically possess morphologies showing the highest symmetry consistent with the chemical and spatial growth constraints imposed. The crystal faces tend to follow the *holohedral*, or *holosymmetric* symmetry, of the crystal class (i.e., they belong to the point group with the highest symmetry of its crystal system). However, as the relatively recently coined terms *crystal engineering* and *grain boundary engineering* (for polycrystalline materials) imply, to attain the optimal properties needed in any given engineering or functional application, it is often desirable—indeed, sometimes necessary—to control morphology (crystal shape, orientation) and/or microstructure (grain size, shape, and texture).

Perhaps the most common scenario is the need to produce crystals with specific crystallographic orientations. For example, large single-crystalline silicon wafers

Inorganic Materials Synthesis and Fabrication, By John N. Lalena, David. A. Cleary, Everett E. Carpenter, and Nancy F. Dean

with particular crystallographic orientations are required for the fabrication of microelectronic devices. The atomic-scale surface topography of each orientation gives rise to a unique interfacial structure between the silicon substrate and films, either deposited or grown thermally. The interface is a significant portion of the total film volume in today's devices, where film thicknesses are in the nanometer range. With metal–oxide semiconductor field-effect transistor (MOSFET) devices, (100)-oriented silicon slices are currently used because they give more reliable gate oxides on thermal oxidation. However, for bipolar devices, the (111) orientation is used.

There are numerous other situations in which particular crystal orientations are required as starting material for the fabrication of devices. For example, high-quality quartz crystals are grown from seeds with specific orientations to maximize the obtainable number of parallelepiped units, called *cuts*, of that particular type for the production of crystal oscillators. The mode of vibration, and hence the corresponding frequency band for which it may be used, is dependent on the unit's crystallographic orientation and thickness, while the angle of the cut relative to the crystal face controls the frequency deviation over a specified temperature range. In a similar fashion, potassium titanyl phosphate, which is widely used for sum frequency generation (e.g., frequency doubling) requires cuts of specific crystallographic orientations that are determined solely by the nonlinear optical process for which it will be used.

Specific crystallographic orientations and symmetry-dependent properties may also be exploited in synthetic schemes in which solids are used as starting materials. Properties and phenomena are facilitated along, or may even be restricted to, specific crystallographic directions or orientations. Examples of anisotropy so utilized include:

- *Transport properties*. Ionic conduction and atomic diffusion are usually easier along certain crystallographic directions or planes.
- *Epitaxial and topotactic controlled reactions*. There are preferred crystallographic orientations for substrates on which single-crystalline films are grown via *homoepitaxy* (the film is the same substance and has the same orientation as the substrate) or heteroepitaxy (the film is a different substance and may have a different orientation than the substrate). Because of lattice matching between reactant and product phases, epitaxial reactions (surface structure controlled), as well as topotactic reactions (bulk crystal structure controlled), proceed under milder synthetic conditions. The kinetic control afforded by the surface step structure in these processes makes possible the obtainment of phases that are thermodynamically metastable but kinetically stable. For example, $YMnO_3$ crystallizes in the hexagonal system at atmospheric pressure, but cubic perovskite films have been grown on $NdGaO_3$ substrates.
- *Chemical activity (functionality)*. Some crystal facets may be significantly more chemically reactive than others. For example, the (100) face of vanadyl

pyrophosphate is active for the oxidation of *n*-butane to maleic anhydride, whereas the other faces are not.

- *Magnetic anisotropy*. In conjunction with slip casting, magnetic alignment of anisotropic particles may be used to produce polycrystalline materials with a preferred orientation, or texture.
- *Plasticity*. Slip, the gliding motion of full planes of atoms or partial planes, called *dislocation*, allows for the deformation processing of polycrystalline metals (forging, extrusion, rolling, swaging, and drawing). Slip occurs much more readily across close-packed planes in close-packed directions.

Because the central topic of this book is synthesis and fabrication, the correlation of crystal *structure* with physical properties is not of primary importance. Nonetheless, as the preceding paragraphs imply, a discussion of the correlation between crystal *symmetry* and physical properties would be wise. The question is: At what point should we make that presentation? Crystal symmetry/physical property correlations were elucidated by physicists in the early to mid-nineteenth century, concurrent with mineralogists' work on the classification of crystals based on geometric form, decades before space group theory and its experimental confirmation by x-ray diffraction made possible crystal structure determination. It therefore seems fitting to place that treatment here, followed by morphological crystallography, the theory of space lattices, surface and interfacial structure, and finally, the crystallographic and morphological considerations pertinent to various preparative routes, which is in roughly the same chronological order as their development.

It must first be recognized that morphological (external) symmetry is not always identical with a specimen's true crystallographic symmetry. As a result, discrepancies between the observed and expected symmetry of a physical property may arise when the symmetry of the crystal is deduced solely from its external appearance. *Consequently, it is more appropriate to deduce the structure and symmetry of a crystal from its physical properties*. An auspiciously unambiguous relationship exists between crystallographic symmetry and physical properties. This principle, which is a basic postulate of crystal physics, was first recognized by Franz Ernst Neumann (1798–1895) in the 1830s (Neumann, 1833) and was later formalized by Neumann's students Woldemar Voigt (1850–1918) and Bernhard Minnigerode (1837–1896) in the 1880s. It may be stated as follows: *The symmetry of a physical phenomenon is* [*at least*] *as high as the crystallographic symmetry*. Similarly, the orientation of the principal axes of the matter tensor representing the physical property must also be consistent with the crystal symmetry (Section 1.1). In addition to physical properties such as electronic and thermal conductivity, mechanical properties such as elasticity, hardness, and yield strength also comply with the crystallographic symmetry.

There are two important points to remember regarding the applicability of Neumann's principle. First, forces *imposed* on a crystal, including mechanical stresses and electric fields, can have any arbitrary direction or orientation. These types

of forces are represented mathematically with field tensors, not matter tensors, and so are not subject to Neumann's principle. Second, Neumann's principle applies strictly to physical properties only. Nevertheless, because of crystalline anisotropy, chemical activity (e.g., oxidation rate, corrosion rate, etch rate) is also found to be either direction- or orientation-dependent. The degree of surface chemical activity generally correlates with the density of bonds (particularly dangling bonds), which, in turn, is influenced by energy-lowering surface reconstructions, a topic we cover in Section 2.3.1.3. For example, the silicon (111) face etches more slowly than, but oxidizes nearly twice as rapidly as, the Si(001) face.

1.1. RELATIONSHIP BETWEEN PHYSICAL PROPERTIES AND CRYSTALLOGRAPHIC SYMMETRY

Neumann's principle asserts that the symmetry elements of any physical property of a crystal must include, at least, all the symmetry elements of the point group of the crystal. Single crystals are generally not isotropic. Hence, the physical properties of single crystals generally will be anisotropic, that is, dependent on the direction in which they are measured. For example, only with cubic crystals or polycrystals possessing a random crystallite orientation are the directions of heat flow (the flux) and the temperature gradient (the driving force) parallel. Accordingly, it is necessary to use mathematical expressions known as *tensors* to explain anisotropic properties in the most precise manner.

A tensor is an object with many components that look and act like components of ordinary vectors. The number of components necessary to describe a tensor is given by p^n, where p is the number of dimensions in space and n is called the *rank*. For example, a zero-rank tensor is a scalar, which has $3^0 = 1$ component regardless of the value of p. A first-rank tensor is a vector; it has three components in three-dimensional space (3^1), the projections of the vector along the axes of some reference frame (e.g., the mutually perpendicular axes of a Cartesian coordinate system). Although the magnitude and direction of a physical quantity, intuitively, do not depend on our arbitrary choice of a reference frame, a vector is defined by specifying its components from projections onto the individual axes of the reference system. Thus, a vector can be defined by the way these components change, or transform, as the reference system is changed by a rotation or reflection. This is called a *transformation law*. For example, a vector becomes the negative of itself if the reference frame is rotated 180°, whereas a scalar is invariant to coordinate system changes (Lalena and Cleary, 2005).

Second-rank tensors such as transport properties relate two first-rank tensors, or vectors. Thus, a second-rank tensor representing a physical property has nine components (3^2), usually written in 3×3 matrixlike notation. Each component is associated with two axes: one from the set of some reference frame and one from the material frame. Three equations, each containing three terms on the right-hand side, are needed to describe a second-rank tensor exactly. For a general

second-rank tensor τ that relates two vectors, **p** and **q**, in a coordinate system with axes x_1, x_2, x_3, we have

$$\begin{aligned} p_1 &= \tau_{11}q_1 \quad \tau_{12}q_2 \quad \tau_{13}q_3 \\ p_2 &= \tau_{21}q_1 \quad \tau_{22}q_2 \quad \tau_{23}q_3 \\ p_3 &= \tau_{31}q_1 \quad \tau_{32}q_2 \quad \tau_{33}q_3 \end{aligned} \tag{1.1}$$

The tensor, with components τ_{ij}, is written in matrixlike notation as

$$\begin{bmatrix} \tau_{11} & \tau_{12} & \tau_{13} \\ \tau_{21} & \tau_{22} & \tau_{23} \\ \tau_{31} & \tau_{32} & \tau_{33} \end{bmatrix} \tag{1.2}$$

Note that each component of **p** is related to all three components of **q**. Thus, each component of the tensor is associated with a pair of axes. For example, τ_{32} gives the component of **p** parallel to x_3 when **q** is parallel to x_2. In general, the number of indices assigned to a tensor component is equal to the rank of the tensor. Tensors of all ranks, like vectors, are defined by their transformation laws. For our purposes, we need not consider these.

Fortunately, several simplifications can be made (Nye, 1957). Transport phenomena, for example, are processes whereby systems transition from a state of nonequilibrium to a state of equilibrium. Thus, they fall within the realm of irreversible or nonequilibrium thermodynamics. *Onsager's theorem*, which is central to nonequilibrium thermodynamics, dictates that as a consequence of time-reversible symmetry, the off-diagonal elements of a transport property tensor are symmetrical (i.e., $\tau_{ij} = \tau_{ji}$). This is known as a *reciprocal relation*. The Norwegian physical chemist Lars Onsager (1903–1976) was awarded the 1968 Nobel Prize in Chemistry for reciprocal relations. Thus, the tensor above can be rewritten as

$$\begin{bmatrix} \tau_{11} & \tau_{12} & \tau_{13} \\ \tau_{12} & \tau_{22} & \tau_{23} \\ \tau_{13} & \tau_{23} & \tau_{33} \end{bmatrix} \tag{1.3}$$

Note the perhaps subtle, but very important, change in subscripts from Eq. 1.2, leaving us with merely six independent components.

Finally, symmetrical tensors can also be diagonalized. For second-rank tensors, three mutually perpendicular unit vectors can be found that define three *principal axes*, such that if these axes are used as coordinate axes, the matrices are diagonal. This leaves

$$\begin{bmatrix} \tau_{11} & 0 & 0 \\ 0 & \tau_{22} & 0 \\ 0 & 0 & \tau_{33} \end{bmatrix} \tag{1.4}$$

Because of this further simplification, only three independent quantities in a symmetrical second-rank tensor are needed to define the magnitudes of the principal components. The other three components (from the initial six), however, are still needed to specify the directions of the axes with respect to the original coordinate system.

In the case of physical properties, crystal symmetry imposes even more restrictions on the number of independent components (Nye, 1957). A tensor representing a physical property must be invariant with regard to every symmetry operation of the given crystal class. Tensors that must conform to the crystal symmetry in this way are called *matter tensors*. The orientation of the principal axes of a matter tensor must also be consistent with the crystal symmetry. The principal axes of crystals with orthogonal crystallographic axes will be parallel to the crystallographic axes. In the monoclinic system, the x and z crystallographic axes are orthogonal to each other but nonorthogonal to y. For triclinc crystals, there are no fixed relations between either the principal axes or crystallographic axes, and no restrictions on the directions of the principal axes. The effects of crystal symmetry on symmetrical second-rank matter tensors are given below.

For cubic crystals and nontextured polycrystals, we have

$$\begin{bmatrix} \tau_{11} & 0 & 0 \\ 0 & \tau_{11} & 0 \\ 0 & 0 & \tau_{11} \end{bmatrix} \tag{1.5}$$

For tetragonal, trigonal, and hexagonal crystals,

$$\begin{bmatrix} \tau_{11} & 0 & 0 \\ 0 & \tau_{11} & 0 \\ 0 & 0 & \tau_{33} \end{bmatrix} \tag{1.6}$$

For orthorhombic crystals,

$$\begin{bmatrix} \tau_{11} & 0 & 0 \\ 0 & \tau_{22} & 0 \\ 0 & 0 & \tau_{33} \end{bmatrix} \tag{1.7}$$

For monoclinic crystals,

$$\begin{bmatrix} \tau_{11} & 0 & \tau_{13} \\ 0 & \tau_{22} & 0 \\ \tau_{13} & 0 & \tau_{33} \end{bmatrix} \tag{1.8}$$

For triclinic crystals,

$$\begin{bmatrix} \tau_{11} & \tau_{12} & \tau_{13} \\ \tau_{12} & \tau_{22} & \tau_{23} \\ \tau_{13} & \tau_{23} & \tau_{33} \end{bmatrix} \tag{1.9}$$

The diagonal elements in the tensors above follow from the indistinguishability of the axes in their respective crystal classes. For example, if we denote the normalized unit length of the three crystallographic axes in each crystal class with the letters a, b, c and denote the angles between these three axes with the Greek letters α, β, γ, we can see that there are three indistinguishable orthonormal dimensions (orthogonal axes normalized to the same unit length) in the cubic class ($a = b = c$; $\alpha = \beta = \gamma = 90^\circ$); two orthonormal dimensions in the tetragonal class ($a = b \neq c$; $\alpha = \beta = \gamma = 90^\circ$); two orthonormal dimensions in the trigonal class ($a = b = c$; $\alpha = \beta = \gamma \neq 90^\circ$); two orthonormal dimensions in the hexagonal class ($a = b \neq c$; $\alpha = \beta = 90^\circ, \gamma = 120^\circ$); no orthonormal dimensions in the orthorhombic class ($a \neq b \neq c$; $\alpha = \beta = \gamma = 90^\circ$); no orthonormal dimensions in the monoclinic class ($a \neq b \neq c$; $\alpha = \gamma = 90^\circ$, $\beta \neq 90^\circ$); and no orthonormal dimensions in the triclinic class ($a \neq b \neq c$; $\alpha \neq \beta \neq \gamma \neq 90^\circ$). The off-diagonal elements in the monoclinic and triclinic crystals give the additional components necessary to specify the tensor. Notice that a cubic single crystal is isometric and so has isotropic properties. The same is also true for polycrystals with a random crystallite orientation (e.g., powders), regardless of the crystal class to which the substance belongs. Thus, a single scalar quantity is sufficient for describing the conductivity in crystals of the cubic class and nontextured polycrystalline materials (Lalena and Cleary, 2005).

It is sometimes possible to use the anisotropy in certain physical properties advantageously during fabrication processes. For example, the magnetic susceptibility, which describes the magnetic response of a substance to an applied magnetic field, is a second-rank matter tensor. It is the proportionality constant between the magnetization of the substance and the applied field strength. When placed in a magnetic field, a crystal with an anisotropic magnetic susceptibility will rotate to an angle in order to minimize the magnetic free-energy density. This magnetic alignment behavior can aid in texture control of ceramics and clays if the particles are sufficiently dispersed to minimize particle–particle interactions, which can be accomplished with slip casting or another powder suspension process (Section 7.3.2). The route has been used to prepare many bulk substances and thin films, including some with only a small anisotropic paramagnetic or diamagnetic susceptibility, such as gadolinium barium copper oxide, zinc oxide, and titanium dioxide (anatase), with textured (grain-aligned) microstructures and correspondingly improved physical properties (Lalena and Cleary, 2005).

1.1.1. Geometrical Representation of Tensors

The components of a symmetrical second-rank tensor, referred to its principal axes, transform like the three coefficients of the general equation of a second-degree surface (a quadric) referred to its principal axes (Nye, 1957). Hence, if all three of the quadric's coefficients are positive, an ellipsoid becomes the geometrical representation of a symmetrical second-rank tensor property (e.g., electrical and thermal conductivity, permittivity, permeability, dielectric and magnetic susceptibility). The ellipsoid has inherent symmetry *mmm*. The relevant features are that (1) it is centrosymmetric, (2) it has three mirror planes perpendicular to the

TABLE 1.1 Relationships Between the Quadric and Crystal Axes for Symmetrical Second-Rank Tensors

Crystal Class	Tensor Components to Be Measured	Restrictions on Principal Directions and Principal Values
Cubic	One value	Principal directions must be parallel to crystal axes; all three principal values equal in magnitude (isotropic)
Tetragonal	Two values	Principal directions must be parallel to crystal axes; two principal values equal in magnitude
Orthorhombic	Three values	Principal directions aligned with crystal axes; no restrictions on values
Hexagonal	Two values	One principal direction aligned with three-fold crystal axis; two principal values equal in magnitude
Trigonal	Two values	One principal direction aligned with three fold crystal axis; two principal values equal
Monoclinic	Three values plus one angle	One principal direction aligned with two-fold crystal axis; no restrictions on values
Triclinic	Three values plus three directions	No restrictions on directions or values; need to measure three directions and three values

principal directions, and (3) its twofold rotation axes are parallel to the principal directions. We have already stated that the orientation of the principal axes of the matter tensor representing a physical property must be consistent with the crystal symmetry. What this means is that the exact shape of the tensor property and its quadric, as well as the orientation of the quadric with respect to the crystal, are all restricted by the crystallographic symmetry. Table 1.1 lists the relationships between the quadric and the crystal axes for the various crystal classes.

1.1.2. Measurement of Physical Properties of Crystals

The most straightforward method for the measurement of a physical property on a single crystal along its principal axes often involves the initial removal of a uniform regularly shaped section (e.g., a parallelepiped or circular disk) from the crystal. This, in turn, usually requires that the single crystal first be oriented, for example, by using a Laue back-reflection technique. Consider the coefficient of thermal expansion (CTE) along the two independent crystallographic axes of a crystal belonging to the tetragonal crystal class, which may be measured using a thermomechanical analyzer (TMA). Measurement of this property is accomplished by first orienting the crystal, followed by cutting out a rectangular parallelepiped specimen (e.g., using a diamond saw blade), and finally, taking the

length change along the crystal axes (a, c) directly from the TMA measurements along both the shorter and longer dimensions of the parallelepiped. Of course, the CTE, as with other intensive properties (which are independent of the mass of the sample) such as conductivity, cannot really be measured directly but rather, must be calculated from measuring the corresponding extensive property.

Often, it is not possible to obtain single crystals that are large enough to be worked with in a convenient manner. In those cases, physical properties must be measured on polycrystalline samples. There is always discrepancy, or disagreement, between measured physical properties of single crystals and polycrystals due to microstructural effects. Hence, physical properties measured from polycrystalline samples are sometimes considered less reliable from a reproducibility standpoint.

1.2. MORPHOLOGICAL CRYSTALLOGRAPHY

Before the advent of diffractometry, crystallographers could only visually examine crystals. However, an entire classification system was developed that is still in use today for describing a crystal's morphology, or external appearance, and for assigning a crystal's external symmetry to a point group. Mineralogists in the early nineteenth century focused on the theory of crystal forms from purely geometrical points of view. Although these systems do not make reference to primitive forms or any other theory of internal structure, they are perfectly valid approaches. The theory of crystal forms was developed independently by Christian Samuel Weiss (1780–1856), professor of geology and mineralogy at the University of Berlin, and by the mineralogist Friedrich Karl Mohs (1773–1839), in 1816 and 1822, respectively. Weiss was able to derive four definite crystal form classes: tessular (isometric, or cubic), pyramidal (tetragonal), prismatic (orthorhombic), and rhombohedral (hexagonal), by choosing as coordinate axes lines drawn joining opposite corners of certain forms. The monoclinic and triclinic systems were considered by Weiss to be hemihedral and tetragonal modifications of the prismatic system, but were considered distinct in Mohs' more advanced treatment (Lalena, 2006).

Weiss and Mohs also developed notation systems relating each face to the coordinate axes, but these were surpassed in use by a system first introduced by the British polymath William Whewell (1794–1866) during a crystallography fellowship period in 1825, and later incorporated in an 1839 book by his student William Hallowes Miller (1801–1880). The notation system, now named after Miller, is discussed further in Section 1.3.2.

Just as there is a correspondence between the symmetry of crystals and that of their physical properties, there is also a connection between the symmetry exhibited by a crystal at the macroscopic and microscopic length scales, in other words, between the "external" crystal morphology and true "internal" crystal structure. Under favorable circumstances, the point group (but not the space group) to which a crystal belongs can be determined solely by examination of

the crystal morphology, without the need of confirmation by x-ray diffraction. It is not always possible because although many crystal forms (a collection of equivalent faces related by symmetry) are normally apparent in a typical crystal specimen, some forms may be absent or show unequal development.

If a crystal is grown in a symmetrical growth environment (e.g., freely suspended in a liquid), its morphological symmetry is exactly that of the isogonal point group (the point group with the same angular relations as that) of the space lattice. Morphological symmetry may depart from the true point group symmetry of the space lattice because of differing intrinsic growth rates of the various faces or because of nonsymmetrical growth conditions (Buerger, 1978). Even the presence of dislocations is believed to influence the growth rates and thus the development of various forms (Dowty, 1976). A comprehensive treatment of geometric crystallography, including morphological and internal symmetry, their interrelationship, and a systematic derivation of all the crystallographic point groups and space groups can be found in Buerger's classic textbook *Elementary Crystallography* (Buerger, 1978).

1.2.1. Single-Crystal Morphology

There are four commonly used terms for describing morphology which should be understood: zone, form, habit, and twin. A *zone* is a volume enclosed by a set of faces that intersect one another along parallel edges. The zone axis is the common edge direction. For example, the crystallographic axes and the edges of a crystal are all zone axes. A crystal *form* is a collection of equivalent faces related by symmetry (e.g., a polyhedron). One can choose the directions of three edges of a crystal as coordinate axes (x, y, z) and define unit lengths (a, b, c) along these axes by choosing a plane parallel to a crystal face that cuts all three axes. For any other crystal face, integers (h, k, l) can be found such that the intercepts the face makes on the three axes are in the ratios $a:h$, $b:k$, $c:l$. Together, these three integers describe the orientation of a crystal face. The integers are prime and simple (small) and they may be positive or negative in sign.

In a cube (a hexahedron), all the faces are equivalent. The six faces have indices (100), (100), (010), (010), (001), and (001), but the set is denoted as {100}, signifying the entire cube, whereas (100) signifies just one face. In a similar fashion, an octahedron has the form symbol {111} and consists of the following eight faces: (111), (111), (111), (111), (111), (111), (111), and (111). One or more crystal forms are usually apparent in the crystal morphology, and these may be consistent with the point group symmetry of the lattice. A crystal of α-quartz (low quartz), for instance, may display five external forms showing trigonal point group symmetry. Symmetry considerations limit the number of possible types of crystal forms to 47. However, when we look at crystals from the lattice-based viewpoint, there are only seven crystal systems. This is because there are 15 different forms, for example, in the cubic (isometric) crystal system alone. The 47 forms are listed in Table 1.2, grouped by the crystal systems to which they belong. Included in the table are representative examples of minerals exhibiting these form developments.

TABLE 1.2 The 47 Possible Forms Distributed Among the Various Crystal Systems

Crystal Class	Symmetry Elements[a]	Forms Occurring in the Respective Crystal Class	Representative Inorganic/Mineral Substances
Triclinic			
$\underline{1}$	E	Pedion	$Ca_8B_{18}Cl_4 \cdot 4H_2O$
$\bar{1}$	E, i	Pinacoid	$MnSiO_3$
Monoclinic			
2	E, C_2	Sphenoid, pedion, pinacoid	$FeAl_2(SO_4)_4 \cdot 22H_2O$
m	E, σ_h	Sphenoid, pedion, pinacoid	$CaMg(AsO_4)F$
$2/m$	E, C_2, I, σ_h	Prism, pinacoid	As_2S_3
Orthorhombic			
222	E, C_2, C_2', C_2'	Disphenoid, prism, pinacoid	$ZnSO_4 \cdot 7H_2O$
$mm2$	E, C_2, σ_v, σ_v	Pyramid, prism, dome, pinacoid, pedion	$BaAl_2Si_3O_{10} \cdot 2H_2O$
mmm	E, C_2, C_2', C_2', σ_v, σ_v, σ_h	Dipyramid, prism, pinacoid	Sulfur
Tetragonal			
$\underline{4}$	E, $2C_4$, C_2	Tetragonal pyramid, tetragonal prism, pedion	None known
$\bar{4}$	E, $2S_4$, C_2	Tetragonal disphenoid, tetragonal prism, pinacoid	$Ca_2B(OH)_4AsO_4$
$4/m$	E, $2C_4$, C_2, i, $2S_4$, σ_h	Tetragonal dipyramid, tetragonal prism, pinacoid	$PbMoO_4$
422	E, $2C_4$, C_2, $2C_2'$, $2C_2''$	Tetragonal trapezohedron, tetragonal dipyramid, ditetragonal prism, tetragonal prism, pinacoid	$Pb_2CO_3Cl_2$
$4mm$	E, $2C_4$, C_2, $2\sigma_v$, $2\sigma_d$	Ditetragonal pyramid, tetragonal pyramid, ditetragonal prism, tetragonal prism, pedion	$Pb_2Cu(OH)_4Cl_2$
$\bar{4}\,2m$	E, C_2, $2C_2'$, $2\sigma_d$, $2S_4$	Tetragonal scalenohedron, tetragonal disphenoid, tetragonal bipyramid, ditetragonal prism, tetragonal prism, pinacoid	Cu_2FeSnS_4

(*continued overleaf*)

TABLE 1.2 (*continued*)

Crystal Class	Symmetry Elements[a]	Forms Occurring in the Respective Crystal Class	Representative Inorganic/Mineral Substances
4/*mmm*	E, $2C_4$, C_2, $2C_2'$, $2C_2''$, i, $2S_4$, σ_h, $2\sigma_v$, $2\sigma_d$	Ditetragonal dipyramid, tetragonal dipyramid, ditetragonal prism, tetragonal prism, pinacoid	Rutile
Trigonal (rhombohedral)			
$\underline{3}$	E, $2C_3$	Trigonal pyramid	$NaIO_4 \cdot 3H_2O$
$\bar{3}$	E, $2C_3$, i, $2S_6$	Rhombohedron, hexagonal prism, pinacoid	$FeTiO_3$
32	E, $2C_3$, $3C_2'$	Trigonal trapezohedron, rhombohedron, trigonal dipyramid, ditrigonal prism, hexagonal prism, trigonal prism, pinacoid	Low quartz
3*m*	E, $2C_3$, $3\sigma_v$	Ditrigonal pyramid, trigonal pyramid, hexagonal pyramid, ditrigonal prism, trigonal prism, hexagonal prism, pedion	$KBrO_3$
$\bar{3}$m	E, $2C_3$, $3C_2'$	Hexagonal scalenohedron, rhombohedron, hexagonal dipyramid, dihexagonal prism, hexagonal prism, pinacoid	Corundum
Hexagonal			
$\underline{6}$	E, $2C_6$, $2C_3$, C_2	Hexagonal prism, pedion	Nepheline
$\bar{6}$	E, $2C_6$, σ_h, $2S_3$	Trigonal dipyramid, trigonal prism, pinacoid	None
6/*m*	E, $2C_6$, $2C_3$, C_2, i, $2S_3$, $2S_6$, σ_h	Hexagonal dipyramid, hexagonal prism, pinacoid	Apatite
622	E, $2C_6$, $2C_3$, C_2, $3C_2'$, $3C_2''$	Hexagonal trapezohedron, hexagonal dipyramid, dihexagonal prism, hexagonal prism, pedion	High quartz

$6mmm$	E, $2C_6$, $2C_3$, C_2, $3\sigma_v$, $3\sigma_d$	Dihexagonal pyramid, hexagonal pyramid, dihexagonal prism, hexagonal prism, pedion	Wurtzite
$\bar{6}$m2	E, $2C_3$, $3C_2'$, σ_h, $2S_3$, $3\sigma_v$	Ditrigonal dipyramid, trigonal dipyramid, hexagonal dipyramid, ditrigonal prism, hexagonal prism, trigonal prism, pinacoid	$BaTiSi_3O_9$
$6/mmm$	E, $2C_6$, $2C_3$, C_2, $3C_2'$, $3C_2''$, i, $2S_3$, $2S_6$, σ_h, $3\sigma_v$, $3\sigma_d$	Dihexagonal dipyramid, hexagonal dipyramid, dihexagonal prism, hexagonal prism, pinacoid	Beryl
Cubic			
23	E, $8C_3$, $3C_2$	Tetartoid, deltohedron, tristetrahedron, pyritohedron, tetrahedron, dodecahedron, cube	$NaBrO_3$
$m3$	E, $8C_3$, $3C_2$, i, $8S_6$, $3\sigma_h$	Diploid, trisoctahedron, trapezohedron, pyritohedron, octahedron, dodecahedron, cube	Pyrite
432	E, $8C_3$, $3C_2$, $6C_2$, $6C_4$	Gyroid, trisoctahedron, trapezohedron, tetrahexahedron, octahedron, dodecahedron, cube	None
$\bar{4}$3m	E, $8C_3$, $3C_2$, $6\sigma_d$, $6S_4$	Hextetrahedron, deltohedron, tristetrahedron, tetrahexahedron, tetrahedron, dodecahedron, cube	Sphalerite
$m3m$	E, $8C_3$, $3C_2$, $6C_2$, $6C_4$, $6\sigma_d$, i, $8S_6$, $3\sigma_h$, $3\sigma_h$, $6S_4$	Hexoctahedron, trisoctahedron, trapezohedron, tetrahexahedron, octahedron, dodecahedron, cube	Diamond

Source: Buerger (1978), pp. 112–168.

[a] E, identity element; i, inversion center; C_n, n-fold proper rotation axis; S_n, n-fold improper rotation (rotoreflection) axis; σ_v, vertical mirror plane (reflection plane contains principal axis); σ_h, horizontal mirror plane (reflection plane perpendicular to principal axis); σ_d, diagonal mirror plane (reflection plane contains principal axis and bisects the angle between the twofold axes normal to the principal axis).

The cube and octahedron are both referred to as *closed forms* because they are comprised of a set of equivalent faces that enclose space completely. All 15 forms in the isometric system, which include the cube and octahedron, are closed. One of the isometric forms, the hexoctahedron, has 48 faces. Six forms have 24 faces (tetrahexahedron, trisoctahedron, trapezohedron, hextetrahedron, gyroid, and diploid). Five forms have 12 faces (dodecahedron, tristetrahedron, pyritohedron, deltahedron, and tetartoid). The final three isometric and closed forms are, perhaps, more familiar to the chemist. These are the tetrahedron (4 faces), cube (6 faces), and octahedron (8 faces). Nonisometric closed forms include the dipyramids (6, 8, 12, 16, or 24 faces), scalenohedrons (8 or 12 faces), the rhombic and tetragonal disphenoids (4 faces), the rhombohedron (6 faces), the ditrigonal prism (6 faces), the tetragonal trapezohedron (8 faces), and the hexagonal trapezohedron (12 faces). *Open forms* do not enclose space. These include the prisms with 3, 4, 6, 8, or 12 faces, parallel to the rotation axis. These parallel faces are equivalent but do not enclose space. Other open (and nonisometric) forms include the pyramid (3, 4, 6, 8, or 12 faces), domes (2 faces), sphenoids (2 faces), pinacoids (2 faces), and pedions (1 face). Open forms may only exist in combination with a closed form or with another open form.

As mentioned earlier, a crystal's external morphology may not be consistent with the true point group symmetry of the space lattice. This may be due to (1) one or more forms being absent or showing anisotropic development of equivalent faces, or (2) the true symmetry of the unit cell simply not being manifested macroscopically upon infinite translation in three dimensions. Let's first consider anisotropic development of faces. The growth rates of faces—even crystallographically equivalent faces and faces of crystals belonging to the isotropic (cubic) crystal class—need not be identical. This may be due to kinetic or thermodynamic factors.

One possible reason is a nonsymmetrical growth environment. For example, the nutrient supply may be blocked from reaching certain crystal faces by foreign objects or by the presence of habit-modifying impurities. Since visible crystal faces correspond to the slow-growing faces, the unblocked faces may grow so much faster that only the blocked faces are left visible where as the fast-growing faces transform into vertices. Consider pyrite, which belongs to the cubic system. Crystal growth relies on a layer-by-layer deposition on a nucleus via an *external* flux of adatom species, which may very well be anisotropic. Hence, unequal development of crystallographically equivalent {100} faces can lead to pyrite crystals exhibiting acicular and platelike morphologies instead of the anticipated cube shape. In fact, not all crystals exhibit distinct polyhedral shapes. Those that do not are termed *nonfaceted crystals*. The word *habit* is used to describe the overall external shape of a crystal specimen. Habits, which can be polyhedral or nonpolyhedral, may be described as cubic, octahedral, fibrous, acicular, prismatic, dendritic (treelike), platy, blocky, or bladelike, among many other terms.

As a second example of a mineral with several possible form developments, let's consider, in a little more detail, quartz (Figure 1.1). Quartz belongs to the symmetry class 32, which has two threefold rotation axes and three twofold axes.

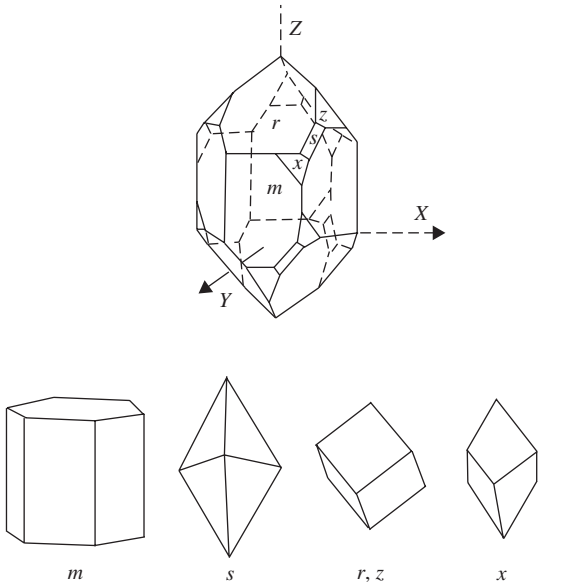

Figure 1.1 Top: Quartz crystal exhibiting the true symmetry of the crystal class to which quartz belongs. Bottom: The forms comprising such a quartz crystal. From left to right, the hexagonal prism, trigonal dipyramid, rhombohedron, and trigonal trapezohedron.

Five forms must necessarily be present to reveal this symmetry: the $\{10\bar{1}0\}$, the $\{10\bar{1}1\}$, the $\{01\bar{1}1\}$, the $\{11\bar{2}1\}$, and the $\{51\bar{6}1\}$. These correspond, respectively, to a hexagonal prism; a dominant, or "positive," rhombohedron; a subordinate, or "negative," rhombohedron; a trigonal (triangular) dipyramid; and a trigonal trapezohedron. In mineralogy, these are labeled, in the order given, with the lowercase letters *m, r, z, s*, and *x*. Three orthogonal crystallographic axes are defined as: *X*, bisecting the angle between adjacent hexagonal prism faces; *Y*, which runs through the prism face at right angles to *X*; and *Z*, an axis of threefold symmetry.

As illustrated in Figure 1.1, both rhombohedra (*r* and *z*) cap, or terminate, the quartz crystal on each end. Each rhombohedron has a set of three faces. By convention, the larger set of three faces is considered the positive rhombohedron. When present, the trigonal trapezohedron (*x*) is seen at the junction of two prism faces (*m*) and the positive rhombohedron and it displays a trapezohedral planar shape. The trigonal pyramid (*s*) is at the junction of the positive rhombohedron and the prism, which is in line vertically with the negative rhombohedron. It typically forms an elongated rhombus-shaped face. However, in some specimens, one or more of the aforementioned forms are missing or show development inconsistent with the true point group symmetry of quartz. In fact, most quartz crystals do not display the trigonal dipyramid or trapezohedron faces, the former being especially rare. With these two forms absent, the rhombohedra may exhibit either equal or unequal development. The latter case implies the highest apparent

(but still false) crystal symmetry, as the hexagonal prism appears to be terminated at both ends with hexagonal pyramids. It is also possible for the hexagonal prism to be absent, in which case the combination of the two rhombohedra results in a hexagonal dipyramid (or bipyramid), termed a *quartzoid*.

We mentioned earlier that the true symmetry of the unit cell may not simply be manifested macroscopically upon infinite translation in three dimensions. Buerger has illustrated this with the mineral nepheline, $(Na,K)AlSiO_4$ (Buerger, 1978). The true symmetry of the nepheline crystal lattice, the symmetry of the unit cell, consists merely of a sixfold rotation axis (class 6) as would be exhibited by a hexagonal prism with nonequivalent halves. That is, there is no mirror plane perpendicular to the rotation axis. However, the absence of this mirror plane is obviously not macroscopically visible in the hexagonal prism form development of nepheline, implying a higher apparent symmetry (6/*mmm*).

The situation with crystallized iodoform, CHI_3, is similar. The molecules are strictly pyramidal, but the crystal contains complementary "positive" and "negative" pyramids capping a hexagonal prism, as do the minerals zinkenite ($Pb_9Sb_{22}S_{42}$) and finnemanite $[Pb_5(AsO_3)_3Cl]$. In fact, no crystals showing form development consistent with class 6 symmetry have been observed. It is observed, rather, that form developments tend to follow the holohedral or holosymmetric symmetry of the crystal class (i.e., the point group with the highest symmetry of its crystal system). This is most commonly manifested by equal development of complementary forms in the merosymmetric classes (i.e., those with less symmetry than the lattice).

Often, the habit assumed by a particular specimen is under kinetic control, being dependent primarily on the growth environment. If crystals grow into one another, as they do in solidification products and polycrystals, it is possible that no forms will be well developed. However, when multiple crystal forms are present, it is possible that some forms (sets of equivalent faces) might have intrinsically higher growth rates than others. Form developments tend to lower the surface energy of the crystal. Surface energy is a function of several parameters:

- The distance of the face from the center of the crystal
- The face orientation, or Miller (*hkl*) indices
- Surface roughness
- The radius of curvature

Under equilibrium growth conditions, the fastest crystal growth will occur in the direction perpendicular to the face with the highest surface energy. As a consequence of this tendency, the total area of high-energy faces is reduced while that of low-energy faces is increased, which effectively results in an overall lowering of the surface energy of the crystal. For nonfaceted crystals, a smaller radius of curvature possesses a higher energy than one with a larger radius of curvature. The effect of surface energy on crystal morphology is discussed in detail in Section 2.3.

Two methods have traditionally been used to rationalize morphology resulting from the differing growth rates of various faces in terms of the lattice symmetry of the crystal. The first is the *Donnay–Harker method* (Donnay and Harker, 1937), which extends the work of Auguste Bravais (1811–1863) and Georges Friedel (1865–1933). The Bravais–Friedel empirical rule (Bravais, 1866; Friedel, 1907) was that the relative morphological importance of crystal forms is in the same order as the concentration of lattice points on their crystal faces, the *reticular density*. The dominant faces represent those planes cutting through the greatest densities of lattice points. Ranking the crystal forms in order of decreasing importance is also equivalent to ranking them in order of increasing reticular area or to decreasing interplanar spacings, which is proportional to the Miller indices of the faces. Hence, those faces with low Miller indices tend to be the morphologically most important. Because the interplanar spacing is the same for all crystal classes in a system, the morphological importance of the various forms tends to follow the holosymmetric symmetry of the system (Buerger, 1978). Joseph D. H. Donnay (1902–1994) and David Harker (1906–1991) later refined the idea to account for all equivalence points, including not only lattice points but also nonlattice sites of identical internal coordinates (Donnay and Harker, 1937). Although it is often successful, the Donnay–Harker method takes no account of atomic arrangement or bonding and is not applicable to the prediction of surface structure (Dowty, 1976).

Bravais rule is an empirical observation, not a scientific law. Recently, it has been proposed that it may, arguably, be viewed as a manifestation of the Curie–Rosen principle of maximum symmetry from information theory, which states that *the degree of symmetry in an isolated system either remains constant or increases as the system evolves*. To understand the relevance of this principle here, it is necessary to define precisely what symmetry is, correlate it with *information entropy*, and establish the link between entropy in information theory and entropy in thermodynamics, which deals with physical nature. Shu-Kun Lin has attempted this (Lin, 1996). Symmetry is regarded as *invariance* of an object when it is subjected, as a whole, to certain transformations in the space of the variables describing it (e.g., rotation, reflection, translation). The degree of symmetry correlates with the degree of *information entropy*, or information loss (Lin, 1996, 2001; Rosen, 1996). For example, a high degree of information entropy is associated with a high degree of similarity. The maximum possible information entropy, indistinguishability (total loss of information), corresponds to perfect symmetry, or highest symmetry, and low orderliness. By contrast, low symmetry corresponds to distinguishability and high orderliness. The principle of maximum symmetry would then seem to imply that crystals should exhibit the highest possible symmetry consistent with the growth constraints imposed. Unfortunately, the link between informational entropy and thermodynamic entropy may only be philosophical; it is still a hotly debated topic. Nevertheless, the principle of maximum symmetry serves as a useful heuristic.

The second, more recent approach at explaining the different rates of growth along different crystallographic directions, addresses all of these aspects, and is

known both as the *Hartman–Perdok theory* and the *periodic bond chain* (PBC) *method* (Hartman and Perdok, 1955a,b,c). It was developed originally by Piet Hartman and Wiepko Gerhardus Perdok (1914–2005), professor of applied crystallography at the University of Groningen, and was built on earlier work by Paul Niggli (1883–1953) and Robert Luling Parker (1893–1973). Hartmann and Perdok showed that crystal structure determines which directions will exhibit rapid growth rates due to a large energy gain which they called the *attachment energy*. As a result of this rapid growth, those faces grow themselves out of existence, becoming "consumed" by the slow-growing faces. In the PBC method, one first identifies infinite stoichiometric chains of atoms connected by strong bonds (the periodic bond chains). These chains do not have dipole moments perpendicular to their crystallographic direction. The strong bonds are the short bonds in the first coordination sphere formed during crystallization. Crystal faces either have two or more PBCs (flat, or F, faces), one PBC (stepped, or S, faces), or none (kinked, or K, faces). The F faces grow the slowest and are thus the morphologically important ones, while the K and S faces grow so quickly they should not be present in the crystal forms. We discuss the PBC method in more detail in Section 4.2.4. For crystal growth to proceed, it is necessary for the surface to capture and incorporate adatoms. Hence, another factor is the availability of surface sites that readily accommodate new growth units. The theory most successful at dealing with this issue is the terrace–ledge–kink (TLK) model, which is discussed further in Sections 1.4.1 and 2.3.1.2.

1.2.2. Twinned Crystals

A *twin* is a symmetrical intergrowth of two or more crystals, or "individuals," of the same substance (Figure 1.2). A *simple twin* contains two individuals; a *multiple twin* contains more than two individuals. The *twin element* is the geometric element about which a twin operation is performed, relating the different individuals in the twin. The twin element may be a reflection plane (*contact twins*) or a rotation axis (*penetration twins*). The twin operation is a symmetry operation for the twinned edifice only, not for the individuals. In *twinning by merohedry*, the twin and the individual lattice point group, as well as their translational symmetry, coincide. If both the point group and translational symmetries of the twin and individual differ, it is referred to as *twinning by reticular merohedry*. Most commonly, twinning is by *syngonic merohedry*, in which the twin operation is a symmetry element of the holohedral point group (one of the seven point groups exhibiting the complete symmetry of the seven crystal systems) while the point group of the individual crystals is a subgroup, exhibiting less then complete (holohedral) symmetry. With *metric merohedry*, the individual lattice has an accidentally specialized metric corresponding to a higher holohedry and a twin operation exists belonging only to the higher holohedry. For example, a twin operation belonging to an orthorhombic lattice may exist for a twinned edifice comprised of two monoclinic crystals. The empirical rule of merohedral twinning was developed originally by Auguste Bravais, François-Ernest Mallard (1833–1894), and, later, Georges Friedel.

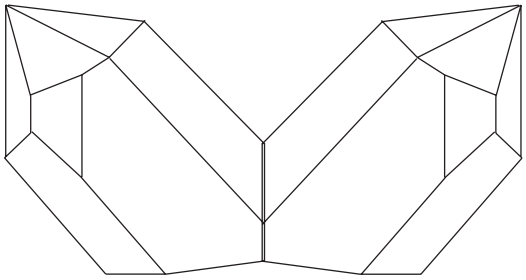

Figure 1.2 "Japan law" contact twin quartz crystal. This type of twinning was discovered in 1829 by C. S. Weiss in quartz crystal from the La Gardette mine in France. However, because of the abundance of these specimens in Japan, they are now known as *Japanese twins*.

Like a grain boundary, the twin boundary is a higher-energy state relative to the crystal. However, because a twin boundary is highly ordered, it is of much lower energy than a typical nontwin grain boundary. Recognizing this, Buerger later proposed that *if the crystal structure is of such a nature that, in detail, it permits a continuation of itself in alternative twin junction configuration, without involving violation of the immediate coordination requirements (the first coordination sphere) of its atoms, the junction has low energy and the twin is energetically possible* (Buerger, 1945).

Twins may also be divided into the following categories based on their origin: *transformation twins* and *growth twins, gliding twins. Growth twins* originate at the nucleation stage under conditions of supersaturation, where there is greater likelihood for the arrival of clusters of atoms, already coordinated, at the twin position. Such twins persist and grow if subsequent clusters of adatoms continue to arrive in that fashion. *Glide twinning* is caused by a specific type of structural shear in plastic deformation. The lower-energy nontwined crystals absorb part of the energy supplied in the plastic deformation process, and if the crystal structure permits it, a layer of atoms glide into a twin position. With continued stress, gliding takes place in the next layer. Because gliding in all the parallel layers does not take place simultaneously, twin lamella form. Calcite is an example of a crystal that forms glide twins readily at low differential stresses ($\sim$10 MPa). Twinning is possible along three glide planes. *Transformation twinning* occurs during the transformation from a high-temperature phase to a lower-symmetry low-temperature phase: for example, when sanidine (monoclinic $KAlSi_3O_8$) is cooled to form microcline (triclinic $KAlSi_3O_8$). In such a process, there is spontaneous formation of nuclei in different orientations, which subsequently grow into one another. Each member of the aggregate is either in parallel or twinned orientation with respect to other members. This follows from the fact that they could be brought into coincidence by one of the possible symmetry operations of the high-temperature phase that vanished in the formation of the low-temperature phase, which has a symmetry that is a subgroup of the high-temperature phase (Buerger, 1945).

Martin Julian Buerger (1903–1986) received his Ph.D. in mineralogy in 1929 from the Massachusetts Institute of Technology MIT, where he remained as an assistant professor. As a graduate student, he attended lectures on x-ray diffraction delivered by W. L. Bragg in 1927, at which point he began his lifelong investigations into crystal structure–property correlation. In the 1930s, Buerger established an x-ray laboratory at MIT, out of which he revised or invented many different types of x-ray cameras and diffractometers as well as carrying out many crystal structure determinations. He also wrote 12 books on crystallography. In addition to being a pioneer in crystal structure analysis, Buerger contributed to a range of other topics within crystallography, crystal growth, polymorphism, twinning, and early (predislocation model) plastic deformation theories. He served as president of both the American Society for X-ray and Electron Diffraction and the Crystallographic Society of America, which later were combined into the American Crystallographic Association. Buerger helped to organize the International Union of Crystallography. He also served as editor-in-chief of *Zeitschrift für. Kristallographie*, and he contributed diagrams, notes, and corrections to the *International Tables of Crystallography*. In 1956, Buerger was the second person to be appointed institute professor at MIT, after John Clarke Slater. He received the Day Medal of the Geological Society of America (1951), the Roebling Medal of the Mineralogical Society of America (1958), and was the first recipient of the Fankuchen Award in 1971. Buerger became university professor emeritus at MIT in 1968 and then accepted an appointment at the University of Connecticut, becoming emeritus there in 1973. The ACA established the triannual *M. J. Buerger Award* in his memory in 1983. Buerger was elected to the U.S. National Academy of Sciences in 1953 and was a member of several foreign academies. He also has a mineral named after him: buergerite, $NaFe_3Al_6(BO_3)_3[Si_6O_{18}]O_3F$.

Source: Obituary by Leonid V. Azároff, *J. Appl. Crystallogr*, **1986**, *19*, 205.

1.2.3. Polycrystalline Texture

Polycrystalline substances, in bulk form and thin films, are composed of crystalline grains, which are sometimes times called *crystallites*. The *microstructure* of a polycrystalline material refers to the crystallite morphology (particle size and shape) and orientation distribution of the grains. The orientation distribution is called *texture*. For example, the grains may all be oriented at random, they may exhibit some preferred orientation (e.g., alignment), or subregions may be present called *domains*, each of which has its own independent orientation. The most common method of illustrating texture is through the use of stereographic projections called *pole figures*, which show the inclination to the normal of a particular crystal plane relative to a reference plane. This is developed much more fully in Section 7.1.1. A succinct discussion can also be found in our companion book, *Principles of Inorganic Materials Design* (Lalena and Cleary, 2005).

As physical properties are anisotropic for all single crystals except for those of the cubic class, texture has important consequences on the symmetry of the physical properties exhibited by polycrystalline materials. It turns out that for a bulk sample containing a sufficiently large number of grains, a completely random grain orientation distribution displays macroscopically isotropic properties as well. Hence, for all cases other than cubic single crystals and nontextured polycrystals, the magnitude of the physical property (e.g., conductivity) will depend on the crystallographic direction. Materials processing is aimed at achieving textures that impart optimal properties for specific design applications.

1.3. SPACE LATTICES

Although the exact morphology (the collection of particular crystal forms, their shapes, and texture) adopted by a specimen is under kinetic control, the number of possible crystal forms is restricted by symmetry, as stated earlier. The number of faces that belong to a form is determined by the symmetry of the point group of the lattice. Put another way, the symmetry of the internal structure *causes* the symmetry of the external *form*s. In this section we consider that internal symmetry in more detail.

Matter is composed of spherical-like atoms. No two atomic cores—the nuclei plus inner shell electrons—can occupy the same volume of space, and it is impossible for spheres to fill all space completely. Consequently, spherical atoms coalesce into a solid with void spaces called *interstices*. A mathematical construct known as a *space lattice* may be envisioned, which is comprised of equidistant lattice points representing the geometric centers of structural motifs. The lattice points are equidistant since a lattice possesses translational invariance. A motif may be a single atom, a collection of atoms, an entire molecule, some fraction of a molecule, or an assembly of molecules. The motif is also referred to as the *basis* or, sometimes, the *asymmetric unit*, since it has no symmetry of its own. For example, in rock salt a sodium and chloride ion pair constitutes the asymmetric unit. This ion pair is repeated systematically, using point symmetry and translational symmetry operations, to form the space lattice of the crystal.

A space lattice may be characterized by its space group symmetry, which consists of point group symmetry (rotations and reflection) and translational symmetry. The morphological symmetry must conform to the angular components of the space group symmetry operations minus the translational components. That is, the symmetry of the external morphology is that of the point group *isogonal* with (possessing the same angular relations as) its space group. It is thus possible under favorable circumstances to determine the point group by an examination of the crystal morphology.

Inorganic solids may be grouped into three structure categories, which are, in the order of decreasing thermodynamic stability: single crystalline, polycrystalline, and amorphous (glassy). Amorphous materials possess no long-range structural order or periodicity. By contrast, a single crystal is composed of a periodic three-dimensional array of atoms or molecules whose positions may be referenced to a lattice, which, as already stated, possesses translational invariance. Some authors also classify recursive patterns known as *fractals* as a distinct structural class. With fractals, the structure is self-similar, looking identical at all length scales. This is a violation of translational invariance and is, in fact, a new type of symmetry called *scale invariance*. Some porous solids (e.g., silica aerogels) have fractal geometry. Many objects in nature (e.g., cauliflower, tree branches, snowflakes, rocks, dendrites) approximate a fractal since the morphologies of their whole are superficially similar to those of the parts comprising them. A polycrystalline material is an aggregate of *crystallites*, or grains, whose lattices exhibit the same translational invariance as their single-crystal counterparts, but the grains are not usually morphologically as well formed. Furthermore, a polycrystalline specimen, as a whole, possesses a *microstructure* that is characterized by the size, shape, and orientation distribution (texture) of the individual crystallites. The atomic-scale structure of the interface between any two crystallites is a function of the relative orientations of the crystallites.

The atoms in a crystalline substance occupy positions in space that can be referenced to *lattice points*, which crystallographers refer to as the *asymmetric unit* (physicists call it the *basis*). Lattice points represent the smallest repeating unit, or chemical point group. For example, in NaCl, each Na and Cl pair may be represented by a lattice point. In structures that are more complex, a lattice point may represent several atoms (e.g., polyhedra) or entire molecules. The repetition of lattice points by translations in space forms a *space lattice*, representing the extended crystal structure.

1.3.1. Two-Dimensional Lattice Symmetry

It is important to study two-dimensional (2D) symmetry because of its applicability to lattice planes and the surfaces of three-dimensional (3D) solids. In two dimensions, a lattice point must belong to one of the 10 point groups listed in Table 1.3 (by the international symbols) along with their symmetry elements. This group, called the *two-dimensional crystallographic plane group*, consists of combinations of a single rotation axis perpendicular to the lattice plane with or

TABLE 1.3 The 10 Two-Dimensional Crystallographic Plane Point Groups and Their Symmetry Elements (International Symbols)[a]

Point Group	Symmetry Elements
Oblique System (Lattice = parallelogram)	
1	1
2	2
Rectangular System (Lattice = Rectangle or Centered Rectangle)	
m	*m*
2*mm*	2, *m* (two perpendicular planes)
Square System (Lattice = Square)	
4	4
4*mm*	4, *m* (two doubly degenerate sets)
Hexagonal System (Lattice = 120° Rhombus)	
3	3
3*m*	3, *m* (triply degenerate set)
6	6
6*mm*	6, *m* (two triply degenerate sets)

[a] *n* (where n = 1, 2, 3, 4, 6), *n*-fold rotation axis perpendicular to the plane; *m* mirror plane (perpendicular to the plane and containing the rotation axis).

without parallel reflection planes (perpendicular to the lattice plane and containing the rotation axis). Note that only those point groups with one-, two-, three-, four-, or sixfold rotations are found in 2D (and 3D) lattices. This can be understood by considering an analogous task of completely tiling a floor with regular polygon tiles. Rhombuses, rectangles, squares, triangles, and hexagons may be used, but not pentagons, heptagons, or higher polygons.

An initial point may be translated in a regular way in two dimensions, thereby generating the *plane lattice*, or *net*, in which each point of the array has exactly the same environment. The points of this plane lattice may be imagined connected together with translation vectors, such that the following equation (in which u and v are integers) holds:

$$\mathbf{R} = u\,\mathbf{a} + v\,\mathbf{b} \tag{1.10}$$

The translation vectors can be chosen so that a *primitive unit cell* is defined that generates the plane lattice when repeated in two-dimensional space. A primitive unit cell of any dimension contains only one lattice point, which is obtained by sharing lattice points at each of its corners with the neighboring unit cells. By convention, the lattice vectors are chosen to be the shortest and most nearly equal as is possible. There are only five unique ways of choosing such translation vectors for a 2D lattice. These are the five *two-dimensional Bravais lattices*, named after the French physicist and mineralogist Auguste Bravais, who derived them in 1850 (Bravais, 1850). The unit cells for each lattice may be described by three parameters: two translation vectors (a, b) and one interaxial angle, usually symbolized as γ. These five lattices (oblique, rectangular, centered-rectangular,

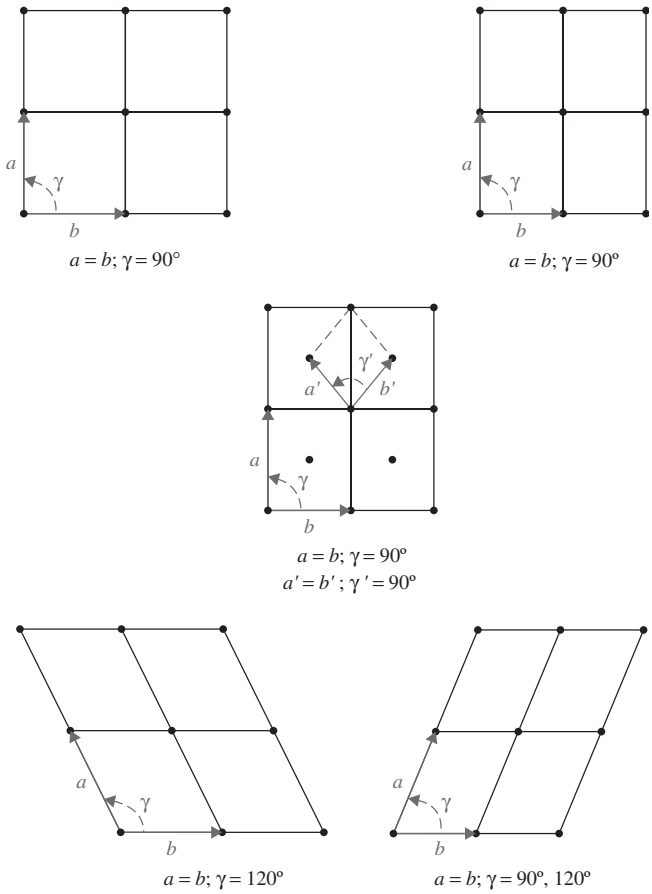

Figure 1.3 Five two-dimensional Bravais lattices. Clockwise from upper left: square, rectangular, oblique, hexagonal, and (center) centered rectangular.

square, and hexagonal) are shown in Figure 1.3. It should be noted that a centered lattice need not be used. An equivalent primitive unit cell can be chosen by defining a new set of nonorthogonal lattice vectors of equal length starting with the same origin and ending on the centered atom, as illustrated in the middle figure. When multiple unit cells are possible, the unit cell with maximum symmetry and smallest area is customarily chosen.

If the 10 point groups allowed are arranged in nonredundant patterns allowed by the five 2D Bravais lattices, 17 unique two-dimensional space groups, called *plane groups*, are obtained (Fedorov, 1891a). Surface structures are usually referred to the underlying bulk crystal structure. For example, translation between lattice points on the crystal lattice plane beneath and parallel to the surface (termed the *substrate*) can be described by an equation identical to Eq 1.10:

$$\mathbf{R} = u'\mathbf{a} + v'\mathbf{b} \tag{1.11}$$

In many cases, the following relation, in which the surface vectors are denoted $\mathbf{a}_s$ and $\mathbf{b}_s$, is found to hold:

$$\mathbf{a}_s = p\mathbf{a} \quad \text{and} \quad \mathbf{b}_s = q\mathbf{b} \tag{1.12}$$

When both p and q are unity, the surface unit cell and the *projection* of the substrate unit cell are the same. This type of surface is designated as 1×1. If both dimensions of the surface's unit cell are twice those of the substrate, the surface is designated 2×2, if only one dimension is n times that of the substrate cell, the surface is $n \times 1$. There are also various "root-three" $\left(\sqrt{3} \times \sqrt{3}\right)$ structures resulting from adsorbed gases on metal surfaces or metals on semiconductor surfaces. The notation for surface structures with adsorbates gets quite complex when rotations relative to the substrate structure are involved. However, we are not concerned with those here.

1.3.2. Three-Dimensional Lattice Symmetry

In an analogous fashion, motifs in three-dimensional lattices must belong to one of the 32 three-dimensional crystallographic point groups, which may be derived by inclusion of the additional symmetry elements found in three-dimensional lattices: namely, centers of inversion, rotoinversion axes, perpendicular reflection planes, and additional axes of rotation. An object that can be replicated to fill all space (a lattice point) in such a way that all the objects so generated are in identical environments (a lattice) can possess only one of these 32 unique combinations of 3D point symmetry, which are the same as the 32 types of external symmetry exhibited by crystals derived by Johann Friedrich Christian Hessel (1796–1872), a physician and professor of mineralogy at the University of Marburg (Hessel, 1830, 1897). These 32 crystallographic point groups and their symmetry elements are listed in the first and second columns of Table 1.2, subdivided into the seven crystal systems. As with 2D nets, only those point groups with one-, two-, three-, four-, or sixfold rotations are found in 3D lattices. The finite number of possible crystallographic point groups also limits the number of external crystal forms to 47.

Equation 1.10, for the translation vectors in a 2D lattice, can be modified in a simple fashion for three dimensions:

$$\mathbf{R} = u\,\mathbf{a} + v\,\mathbf{b} + w\,\mathbf{c} \tag{1.13}$$

In direct analogy with two dimensions, we can define a *primitive unit cell* that when repeated by translations in space, generates a 3D space lattice. There are only 14 unique ways of connecting lattice points in three dimensions, which define unit cells (Bravais, 1850). These are the 14 *three-dimensional Bravais lattices*. The unit cells of the Bravais lattices may be described by six parameters: three translation vectors (a, b, c) and three interaxial angle (α, β, γ). These six parameters differentiate the seven crystal systems: triclinic, monoclinic, orthorhombic, tetragonal, trigonal, hexagonal, and cubic.

There are 230 3D *space groups*, obtained by arranging the 32 crystallographic point groups in the patterns allowed by the 14 3D Bravais lattices. This was shown independently, using different methods, by the British crystallographer William Barlow (1845–1934), the Russian mathematician Evgraf Stepanovich Fedorov (1853–1919), and the German mathematician Arthur Moritz Shönflies (1853–1928) (Fedorov, 1891b; Schönflies, 1891; Barlow, 1894). It was once believed that geometric crystallography was a "closed" or "dead" science, since all possible crystallographic point groups and space groups had been derived. However, the discovery in the 1980s of *quasicrystalline* solids that contain five-, eight-, 10-, and 12-fold rotational symmetry seems to have changed that view.

The notation system developed by Schönflies for designating point group symmetry (Table 1.3) is still widely used by spectroscopists. However, crystallographers use the *Hermann–Mauguin*, or *International*, *notation* for space group symmetry. This system was developed by Carl Hermann (1898–1961) and Charles Mauguin (1878–1958) (Hermann, 1928, 1931; Mauguin, 1931). Each space group is isogonal with one of the 32 crystallographic point groups. However, space group symbols reveal the presence of two additional symmetry elements, formed by the combination of point group symmetry (proper rotations, improper rotations, and reflection) with the translational symmetries of the Bravais lattices. The two types of combinational symmetry are the *glide plane* and *screw axis*. The first character of an international space group symbol is a capital letter designating the Bravais lattice centering type (primitive = P; all-face-centered = F; body-centered = I; face-centered = C, A; rhombohedral = R). This is followed by a modified point group symbol giving the symmetry elements (axes and planes) that occur for each of the lattice symmetry directions for the space group (Lalena, 2006).

Within the unit cell, atoms may be located at *general positions* or, if they lie on a symmetry element (inversion center, rotation axis, mirror plane), at *special positions*. A general position is left invariant only by the identity operation. Each space group has only one general position but the position may have multiple equivalent coordinates. For example, for a phase crystallizing in the space group *Pmmm*, an atom located in the general position x,y,z will, by symmetry, also be found at seven other coordinates: $-x,-y,z$; $-x,y;-z$; $x,-y;-z$; $-x,-y,-z$; $x,y,-z$; $x,-y,z$; and $-x,y,z$. The general position is said to have a *multiplicity* of eight. For primitive cells, the multiplicity of the general position is equal to the order of the point group of the space group; for centered cells, the multiplicity is equal to the product of the order of the point group and the number of lattice points per cell (Lalena, 2006).

A set of symmetry-equivalent coordinates is said to be a special position if each point is mapped onto itself by one other symmetry operation of the space group. In the space group *Pmmm*, there are six unique special positions, each with a multiplicity of four, and 12 unique special positions, each with a multiplicity of two. If the center of a molecule happens to reside at a special position, the molecule must have at least as high a symmetry as the site symmetry of the special position. Both general and special positions are also called *Wyckoff*

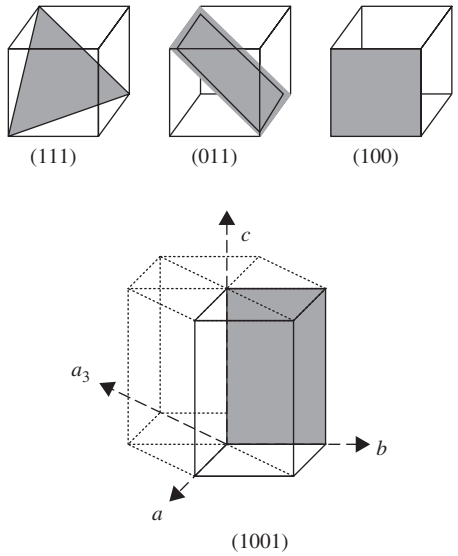

Figure 1.4 Examples of lattice planes and their Miller indices. (After Lalena and Cleary, 2005. Copyright © John Wiley & Sons, Inc. Reproduced with permission.)

positions, in honor of the American crystallographer Ralph Walter Graystone Wyckoff (1897–1994). Wyckoff's 1922 book, *The Analytical Expression of the Results of the Theory of Space Groups*, contained tables with the positional coordinates, both general and special, permitted by the symmetry elements. This book was the forerunner of *International Tables for X-ray Crystallography*, which first appeared in 1935 (Lalena, 2006).

Often, it is necessary to refer to a specific family of lattice planes or a direction in a crystal. A family of lattice planes is a set of imaginary parallel planes that intersect the unit cell edges. Each family of planes is identified by its Miller indices. The Miller indices are the reciprocals of the fractional coordinates of the three points where the first plane away from the origin intercepts each of the three axes. The letter h refers to the intersection of the plane on a; k the intersection on b; and l the intersection on c. Some examples are illustrated in Figure 1.4. These indices are the same as those introduced earlier for denoting the external faces of crystals. When referring to a specific plane in a family, the numbers are grouped together in parentheses, (hkl). Any family of planes always has one member that passes through the origin of the unit cell. The plane used in determining the Miller indices is always the first one away from the origin, which may be obtained by moving in either direction.

Note that a Miller index of zero implies that the plane is parallel to that axis, since it is assumed that the plane will intersect the axis at $1/\infty$. A complete set of equivalent planes is denoted by enclosing the Miller indices in braces: {hkl}. For example, cubic systems (100), ($\bar{1}$00), (010), (0$\bar{1}$0), (001), and (00$\bar{1}$) are equivalent and the set is denoted as {100}. The maximum possible number

of (hkl) combinations that are equivalent occurs for cubic symmetry and is 48. In hexagonal cells, four indices are sometimes used, $(hkil)$, where the relation $h + k + i = 0$ always holds. The value of the i index is the reciprocal of the fractional intercept of the plane on the a_3 axis, as illustrated in Figure 1.4. It is derived in exactly the same way as the others. Sometimes, hexagonal indices are written with the i index as a dot, and in other cases it is omitted entirely.

To specify a crystal direction, a vector is drawn from the origin to a point P. This vector will have projections u' on the **a** axis, v' on the **b** axis, and w' on the **c** axis. The three numbers are divided by the highest common denominator to give the set of smallest integers, u, v, and w. The direction is then denoted $[uvw]$. Sets of equivalent directions are labeled uvw. For cubic systems, the $[hkl]$ direction is always orthogonal to the (hkl) plane of the same indices.

1.4. SURFACE AND INTERFACE STRUCTURES

We assume in the following discussion that the solid surface under consideration is of the same chemical identity as the bulk, that is, free of any oxide film or passivation layer. Crystallization proceeds at the interfaces between a growing crystal and the surrounding phase(s), which may be solid, liquid, or vapor. Even what we normally refer to as a crystal "surface" is really an interface between the crystal and its surroundings (e.g., vapor, vacuum, solution). An *ideal surface* is one that is the perfect termination of the bulk crystal. Ideal crystal surfaces are, of course, highly ordered since the surface and bulk atoms are in coincident positions. In a similar fashion, a *coincidence site lattice* (CSL), defined as the number of coincident lattice sites, is used to describe the goodness of fit for the crystal–crystal interface between grains in a polycrystal. We'll return to that topic later in this section.

1.4.1. Surface Structure

Again, we assume that the solid surface in question is untarnished. Even so, most surfaces are not ideal. They undergo energy-lowering processes known as *relaxation* or *reconstruction*. The former process does not alter the symmetry, or structural periodicity, of the surface. By contrast, surface reconstruction is a surface symmetry-lowering process. With reconstruction, the surface unit cell dimensions differ from those of the *projected* crystal unit cell. It will be recalled that a crystal surface must possess one of 17 two-dimensional space group symmetries. The bulk crystal, on the other hand, must possess one of 230 space group symmetries.

The *terrace–ledge–kink* (TLK) *model* (Kossel, 1927; Stranski, 1928) is commonly used to describe equilibrium solid surfaces. This model was proposed by the German physicist Walther Kossel (1888–1956), who had contributed to the theory of ionic bonding earlier in the century, and by the Bulgarian physical chemist Iwan Nicholá Stranski (1897–1979). It categorizes ideal surfaces or

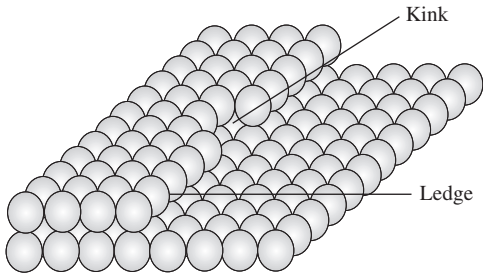

Figure 1.5 Atomic-scale illustration of the terrace–ledge–kink (TLK) model. The top partial layer of spheres represent a terrace, and the bottom layer, the underlying surface atoms.

interfaces as singular, vicinal, and general. An interface is regarded as *singular* with respect to a degree of freedom if it is at a local minimum of energy with respect to changes in that degree of freedom. A *vicinal* interface, by contrast, possesses an interfacial free energy *near* a local minimum with respect to a degree of freedom. A *general* interface, on the other hand, is not at a minimum of energy with respect to any of its degrees of freedom.

Singular surfaces tend to have dense, relatively close packed atomic planes in the crystalline phase parallel to the surface plane and are thus nominally flat. Singular faces have low energy and low entropy. With vicinal surfaces (Figure 1.5), the surface is inclined at a small angle to a low-index plane. Consequently, vicinal surfaces consist of flat two-dimensional one-atom-thick steps of constant width called *terraces*, the edges of which are called *ledges*. Additionally, *kinks*, caused by the removal of atoms in the ledges, are usually present.

A screw dislocation that intersects a crystal surface, termed a *Frank source* after British physicist Sir Charles Frank (1911–1998), is one way in which a surface step may be introduced on real surfaces. In Section 2.5.1 we will see that vicinal surfaces grow layerwise by step propagation, the terraces advancing by the motion of the ledges, which provide preferred binding sites for adatoms. In the case of the Frank source, adatoms attach around the existing screw dislocation, creating an initial double step, which grows in an Archimedean spiral pattern (Burton et al., 1951), as illustrated in Figure 1.6. The Burton–Cabrera–Frank (BCF) model of spiral growth has been applied to a variety of substances, including epitaxially grown semiconductor GaAs films, pyroelectric triglycine sulfate crystals, and amino acids crystallized from solution. Recently, strain fields of dislocations at the surface of Si(001) films have been engineered to nucleate Ge quantum dots preferentially at specific surface locations (Hannon et al., 2006).

1.4.2. Solid–Vapor and Solid–Liquid Interfacial Structures

We can specify the thickness of the crystal interface as that depth over which the structural order of the crystal transitions to that of the surrounding phase(s). On the solid side of the interface, the depth can vary from one lattice spacing for ordered interfaces to several lattice spacings for disordered surfaces

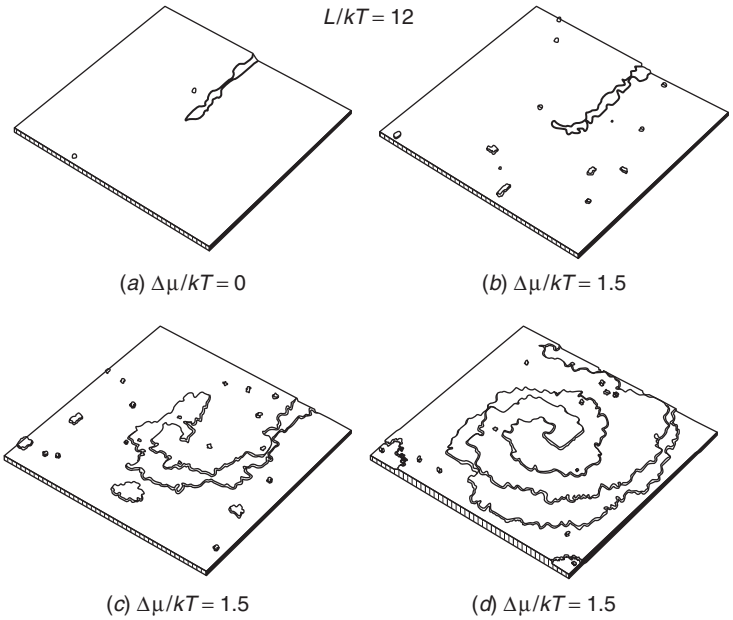

Figure 1.6 The presence of a screw dislocation provides an initial step for the spiral growth pattern illustrated in this early Monte Carlo simulation. (After J. D. Weeks and G. H. Gilmer, *Advances in Chemical Physics*. Copyright © 1979 John Wiley & Sons, Inc. Reproduced with permission.)

and interfaces. Ordered interfaces are typically observed in crystal growth from solutions. Disordered interfaces are much more diffuse, being several lattice spacings thick, and thus exhibiting a more gradual transition from the long-range order of the crystal lattice to the incoherency of the liquid or gas. Such "rough" interfaces are common in solidification (molten phase) processes used for the production of polycrystalline metals and alloys. The liquid phase itself at a solid–liquid interface exhibits crystal-induced structural ordering. The liquid's molecules tend to arrange in layers parallel to the solid surface, which, owing to its atomic-scale corrugation, produces density modulations in the liquid along the direction perpendicular to the solid surface. In general, our understanding of interfacial structure between particles in condensed phases (solid–liquid and solid–solid) is much less developed than that of solid–vapor interfaces. This is partly due to the difficulty associated with experimentally probing "buried" interfaces.

1.4.3. Solid–Solid Interfacial Structure

The modern method for quantifying the goodness of fit between two adjacent grains in a pure polycrystalline substance (homophase interfaces) or in a multiphase solid (heterophase interfaces) counts the number of lattice points (*not*

atomic positions) in each grain that coincide. In special cases, for example when the grain boundary plane is a twin plane, the lattice sites for each of the adjacent crystals coincide *in* the boundary. These are called *coherent boundaries*. Consider a pair of adjacent crystals. We mentally expand the two neighboring crystal lattices until they interpenetrate and fill all space. Without loss of generality, it is assumed that the two lattices possess a common origin. If we now hold one crystal fixed and rotate the other, it is found that a number of lattice sites for each crystal, in addition to the origin, coincide with certain relative orientations. The set of coinciding points form a *coincidence site lattice* (CSL), which is a sublattice for both individual crystals (Lalena and Cleary, 2005).

To quantify the lattice coincidence between the two grains, A and B, the symbol Σ customarily designates the reciprocal of the fraction of A (or B) lattice sites that are common to both A and B:

$$\sum = \frac{\text{number of crystal lattice sites}}{\text{number of coincidence lattice sites}} \tag{1.14}$$

For example, if one-third of the A (or B) crystal lattice sites are coincidence points belonging to both the A and B lattices, then $\Sigma = 1/\frac{1}{3} = 3$. The value of Σ also gives the ratio between the areas enclosed by the CSL unit cell and crystal unit cell. The value of Σ is a function of the lattice types and grain misorientation. The two grains need not have the same crystal structure or unit cell parameters. Hence, they need not be related by a rigid body rotation. The boundary plane intersects the CSL and will have the same periodicity as that portion of the CSL along which the intersection occurs (Lalena and Cleary, 2005).

The simple CSL model is directly applicable to the cubic crystal class. The lower symmetry of the other crystal classes necessitates the more sophisticated formalism known as the *constrained coincidence site lattice*, or CCSL (Chen and King, 1988). In this book we treat only cubic systems. Interestingly, whenever an *even* value is obtained for Σ in a cubic system, it will always be found that an additional lattice point lies in the center of the CSL unit cell. The true area ratio is then half the apparent value. This operation can always be applied in succession until an odd value is obtained: thus, Σ is always *odd* in the cubic system. A rigorous mathematical proof of this would require that we invoke what is known as *O-lattice theory* (Bollman, 1967). The O-lattice takes into account all equivalence points between two neighboring crystal lattices. It includes as a subset not only coinciding lattice points (the CSL) but also all nonlattice sites of identical internal coordinates. However, expanding on that topic would take us well beyond the scope of this book. The interested reader is referred to Bhadeshia (1987) or Bollman (1970).

Single crystals and bicrystals with no misorientation (i.e., $\theta = 0$) are, by convention, denoted $\Sigma 1$. In practice, small- or low-angle grain boundaries with a misorientation angle less than 10 to 15° are also included under the $\Sigma 1$ term. Since Σ is always odd, the coincidence orientation for high-angle boundaries with the largest fraction of coinciding lattice points is $\Sigma 3$ (signifying that one-third of the lattice sites coincide). Next in line would be $\Sigma 5$, then $\Sigma 7$, and so on.

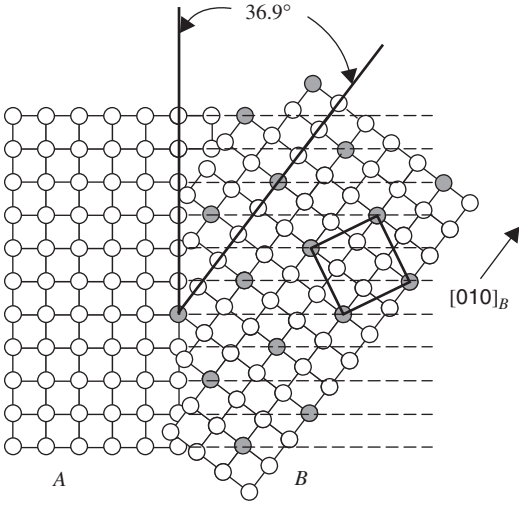

Figure 1.7 View down the [001] direction of a tilt boundary between two crystals (*A*, *B*) with a misorientation angle of 36.9° about [001]. The grain boundary is perpendicular to the plane of the page. Every fifth atom in the [010] direction in B is a coincidence point (shaded). The area enclosed by the CSL unit cell (bold lines) is five times that of the crystal unit cell, so $\sum = 5$. (After Lalena and Cleary, 2005. Copyright © John Wiley & Sons, Inc. Reproduced with permission.)

Figure 1.7 shows a tilt boundary between two cubic crystals. The grain boundary plane is perpendicular to the plane of the page. In the figure we are looking down one of the ⟨100⟩ directions, and the [100] axis about which grain *B* is rotated is also perpendicular to the page and passes through the origin. At the precise misorientation angle of 36.9°, one-fifth of the *B* crystal lattice sites are coincidence points, which also belong to the expanded lattice of crystal *A*; this is a Σ5 CSL misorientation. The set of coincidence points forms the coincidence site lattice, the unit cell of which is outlined. Note that the area enclosed by the CSL unit cell is five times that enclosed by the crystal unit cell.

For tilt boundaries, the value of Σ can also be calculated if the plane of the boundary is specified in the coordinate systems for both adjoining grains. This method is called the *interface-plane scheme* (Wolfe and Lutsko, 1989). In a crystal, lattice planes are imaginary sets of planes that intersect the unit cell edges. The tilt and twist boundaries can be defined in terms of the Miller indices for each of the adjoining lattices and the twist angle, Φ, of both plane stacks normal to the boundary plane, as follows:

$(h_1k_1l_1) = (h_2k_2l_2)$;	$\Phi = 0$	symmetric tilt boundary
$(h_1k_1l_1) \neq (h_2k_2l_2)$;	$\Phi = 0$	asymmetric tilt boundary
$(h_1k_1l_1) = (h_2k_2l_2)$;	$\Phi > 0$	low-angle twist boundary
$(h_1k_1l_1) \neq (h_2k_2l_2)$;	$\Phi > 0$	high-angle twist boundary

Thus, the value of the CSL-Σ value is obtained for symmetric tilt boundaries between cubic crystals as follows:

$$\sum = \begin{cases} h^2 + k^2 + l^2 & \text{for } h^2 + k^2 + l^2 = \text{odd} \\ \frac{h^2 + k^2 + l^2}{2} & \text{for } h^2 + k^2 + l^2 = \text{even} \end{cases} \tag{1.15}$$

For asymmetric tilt boundaries between cubic crystals, Σ is calculated from (Randle, 1993)

$$\sum = \sqrt{\frac{h_1^2 + k_1^2 + l_1^2}{h_2^2 + k_2^2 + l_2^2}} \tag{1.16}$$

For example, it can be shown that in Figure 1.7 the grain boundary plane cuts the B unit cell at (340) in the B coordinate system and the A unit cell at (010) in the A coordinate system. Thus, Eq. 1.16 yields $\Sigma = (25/1)^{1/2} = 5$.

In polycrystals, misorientation angles rarely correspond to *exact* CSL configurations. There are ways of dealing with this deviation, which set criteria for the proximity to an exact CSL orientation that an interface must have to be classified as belonging to the class $\Sigma = n$. The Brandon criterion (Brandon et al., 1964) asserts that the maximum deviation permitted is $v_0 \Sigma^{-1/2}$. For example, the maximum deviation that a $\Sigma 3$ CSL configuration with a misorientation angle of 15° is allowed to have and still be classified as $\Sigma 3$ is $15^\circ(3)^{-1/2} = 8.7^\circ$. The coarsest lattice characterizing the deviation from an exact CSL orientation, which contains the lattice points for each of the adjacent crystals, is referred to as the *displacement shift complete* (DSL) *lattice*.

Despite the difficulties associated with characterizing inexact CSL orientations, the CSL concept is useful because grain boundary structure, which depends on the orientation relationship between the grains and hence the CSL, directly influences intragranular properties such as chemical reactivity (e.g., corrosion resistance), segregation, and fracture resistance. *Grain boundary engineering* is a relatively new field that concentrates on controlling the intragranular structure, or CSL geometry, to improve these properties: in turn, improving bulk materials performance (Watanabe, 1984, 1993). For the most part, this means introducing a large fraction of low-Σ boundaries, particularly twin boundaries. It is believed, however, that optimal grain boundary properties may be restricted to narrow regions (small deviations) about exact CSL orientations (Lalena and Cleary, 2005).

1.5. CONTROLLED CRYSTAL GROWTH AND MICROSTRUCTURAL EVOLUTION

Consistently reliable approaches for the de novo prediction of a material's crystal structure (unit cell shape, size, and space group), morphology (external symmetry), microstructure, as well as its physical properties, remain elusive for

molecular and nonmolecular materials. Nevertheless, empirical synthetic guidelines do exist for preparing general single-crystal morphologies and polycrystalline microstructures, even though we are far from capable of reproducing the vast number of morphologies and degrees of perfection nature has produced. Nonmolecular and molecular materials are often prepared by conventional crystallization processes from, respectively, melts or solutions. Crystallization from a liquid melt phase with the same chemical identity as the solid produced is normally termed *solidification*. Crystallization processes from a liquid solvent include those from homogeneous supersaturated solutions and the low-temperature processes known as the *sol–gel, hydrothermal*, and *solvothermal techniques*. A relative newcomer to materials science and engineering is self-assembly. Now we discuss the crystallographic and morphological control attainable with all the crystallization processes and self-assembly processes, which makes these strategies attractive approaches to materials synthesis.

1.5.1. Conventional Crystallization from Melts and Solvents

There are many analogies between the crystallization process from a molten state and from a solvent. These are discussed fully in Chapter 4. It is often desirable for us to assist the growth of a particular face of a single-crystalline material. For example, as mentioned earlier, because of the desirable properties displayed by certain crystallographic planes in silicon and other semiconductors (e.g., GaAs, InSb, CdTe) exceedingly high-purity single-crystalline substrates with precise orientations are used in microelectronic devices. Such substrates are obtained from oriented single-crystalline ingots, or boules, which may be produced by a variety of solidification processes to be introduced shortly. These and other conventional crystal growth methods are discussed in more detail in subsequent chapters.

In general, the task of controlling single-crystal growth along certain directions may be relatively simple or, conversely, more difficult, depending on the crystal growth method used and the preferential growth directions of the crystal. Defect-free morphologically flawless crystals are rarely found in nature. The quartz crystals used as crystal oscillators, for example, are therefore produced by a *hydrothermal recrystallization* process. In fact, C. E. Schafhäult prepared tiny synthetic, or "cultured," quartz crystals hydrothermally as early as 1845. Hydrothermal chemical synthesis of phases from precursors is also possible, which we discuss in Section 4.4.

To obtain single crystals by hydrothermal recrystallization, a *charge*, which consists of fragments of natural quartz crystals, is dissolved in a solvent, such as 0.5 to 1.0 molar alkaline aqueous solution of sodium carbonate or sodium hydroxide, in the dissolving chamber of an autoclave under high temperature and pressure ($\sim$340 to 380°C, 70 to 150 MPa). Under these conditions, of course, the solution vaporizes. An oriented seed crystal (generally Y-bar or Z-plate with a long [1010] direction) is hung in the upper region above the solution, called the *growing chamber*, which is separated from the lower chamber by a metal baffle.

The growing chamber is maintained at a lower temperature than the dissolving chamber ($\Delta T = \sim 10$ *to* 40°C, depending on the pressure). The temperature difference inside this closed cylinder of fluid results in a vertical, closed-loop heat convection pattern that forces the less dense warm fluid to rise, thus constituting what is called a *phase-change thermosyphon*. Because the growing chamber is at a lower temperature, that region becomes supersaturated and the quartz deposits, or recrystallizes, on the seed. Quartz crystals of over 1500 kg mass, taking over a month to obtain, are produced routinely in this manner in industry. After growth, a diamond saw is used to cut sections from the quartz crystal for use as crystal oscillators, a very laborious task!

The primary experimental parameter affecting growth rate is ΔT, but growth rate is also influenced by the pressure as well as solvent type and concentration. As explained in Section 1.2.1, the growth rate is asymmetric for the various crystal faces. For example, in the early stages of the growth process, the faces of the trigonal trapezohedra (Figure 1.1) become inhibited by those of the hexagonal prism. Even crystallographically equivalent faces (e.g., x) may have different growth rates, due to differing levels of impurity segregation or surface adsorption of vapor species, which act as growth-rate inhibitors.

Other crystal growth methods, where a seed crystal is in physical contact with a high-temperature melt under ambient pressure, include the *submerged-seed solution growth* (SSSG) process, sometimes called *volumetric growth*; and the *top-seeded solution growth* (TSSG) process, in which the seed just touches the melt surface. These methods have been used to chemically synthesize single crystals from metal oxide precursors: for example, calcium-doped yttrium barium copper oxide (YBCO) from Y_2O_3, $BaCO_3$, $CaCO_3$, and CuO, with MgO as the seed (Lin et al., 2002), and <001> seed-oriented potassium titanyl phosphate (KTP) from KH_2PO_4, TiO_2, and K_2HPO_4 (Kannan et al., 2002).

In TSSG, the product crystallizes on the seed as it is pulled away from the constant-temperature melt surface or, alternatively, as the melt is slowly cooled (0.5 to 2 K/day), while maintaining a temperature gradient between the bottom of the crucible and the melt surface. In the crystal pulling version, the pulling shaft may be cooled internally, which maintains the melt surface at a slightly lower temperature than the melt at the bottom of the crucible and allows for heat convection transport. The crucible and the seed may also be rotated in opposite directions to prevent secondary nucleation from heat convection. The growth habit of the synthetic crystals produced from TSSG, which typically produces fewer morphologically developed crystal faces than are produced by SSSG, can be varied by changing the process conditions and/or the size and orientation of the seed crystal. Finally, to obtain large single crystals from incongruent melts, as in Ca-doped YBCO and KTP growth, it is important to keep the melt supersaturated and to apply an extremely slow growth rate, typically around 1 mm/day (Lin et al., 2002).

A very important industrial crystallization process, which is the most common method used for the production of high-purity oriented single-crystalline semiconductor ingots, is the *Czochralski method* (Czochralski, 1918), named

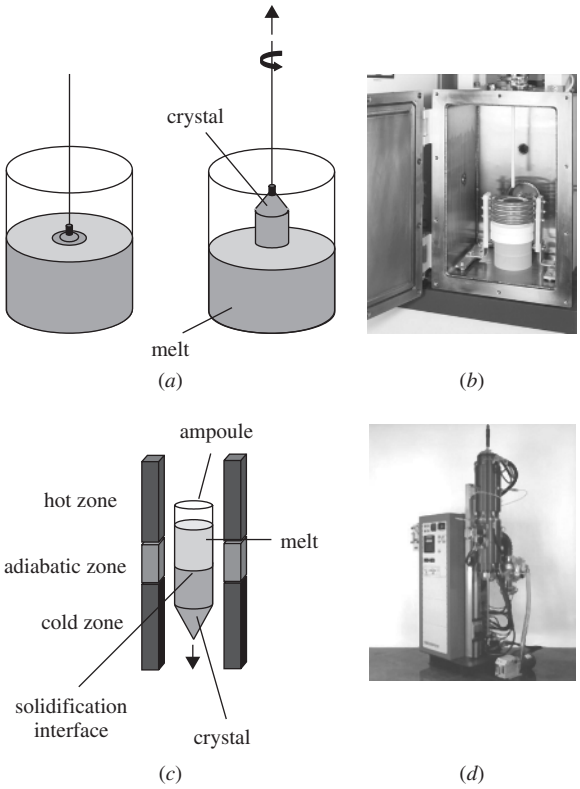

Figure 1.8 (*a*) Czochralski crystal pulling technique; (*b*) commercial Czochralski crystal growth system; (*c*) Bridgman crystal growth technique; (*d*) Bridgman crystal growth laboratory furnace. (Courtesy of Thermal Technology Incorporated, Santa Clara, CA.)

after metallurgist Jan Czochralski (1885–1953) and illustrated in Figure 1.8*a*. A single-crystal dislocation-free seed, or nucleus, with the desired orientation is placed over a congruent melt held at a temperature close to the liquid–solid phase transition. After dipping the seed crystal in the melt, it is pulled upward under continuous rotation. The cylindrical axis of the ingot coincides with the desired crystal growth axis (e.g., silicon ⟨001⟩ or ⟨111⟩). Slices, called *wafers*, on which the microelectronic devices are fabricated are then sawed from the ingot. Semiconductor crystal growth is indeed a very important industrial process, but it should be realized that the Czochralski method is not limited to the growth of oriented semiconductor ingots. It has been used to grow ruby, sapphire, spinel, yttrium–aluminum–garnet (YAG), gadolinium–gallium–garnet (GGG), alexandrite, and $La_3(Ga,Ta)_6O_{14}$, among others. However, it is not suitable for growing crystals from incongruently melting substances.

It is also possible to produce single-crystal ingots as well as highly oriented textured polycrystalline materials (i.e., those in which the grains exhibit a preferred orientation) by directional solidification. With the *Bridgman technique*

(Bridgman, 1926), named after its inventor, Nobel laureate Percy Williams Bridgman (1882–1961), the solidification interface is advanced from a seed crystal into the melt as shown in Figure 1.8*c*. This is accomplished by first placing the substance inside the hot zone of a furnace with a prescribed temperature gradient to create a melt and then gradually moving the melt into the cooler end to induce crystallization. In the modified *Stockbarger method* (Stockbarger, 1936), named after Donald C. Stockbarger (1895–1952), the isothermal hot and cold zones are separated by an adiabatic zone created by an insulating baffle designed to maintain a steep axial temperature gradient. The charge is gradually moved through the adiabatic zone so that the solidification interface remains essentially parallel with the plane of the baffle. It should be noted that the Bridgman method may be utilized in a vertical or horizontal fashion. However, it is necessary to use ampoules that do not bond to the crystal when it freezes. In the case of silicon, none are available. For gallium arsenide, fused silica is satisfactory (Runyan and Bean, 1990).

It is also possible to obtain polycrystalline materials, with grains on the order of millimeters to centimeters in width, at the cooler end in directional solidification techniques. The grains are approximately columnar along the direction of the temperature gradient. The longitudinal axis of the columnar grains corresponds to the direction of highest growth rate in the material. Columnar grains emerge from the sites of preferred nucleation at the cold mold walls and grow in the direction of the highest temperature gradient. Even in conventional casting, where a melt is poured into a mold of some desired shape and size to solidify, there is normally a columnar zone in the center of the cast where elongated crystals with a preferred growth direction have eliminated the randomly oriented grains near the cooler mold walls (the equiaxed zone). The texture can thus be interpreted in terms of a growth selection process: Random nucleation takes place at the mold walls. During the subsequent solidification, selective growth of grains with a specific crystal direction parallel to the highest temperature gradient or heat flow occurs. Consequently, when one examines the microstructures of polycrystalline materials obtained by most industrial solidification processes, it is often found that the individual grains (crystallites) are not morphologically similar to naturally occurring single crystals of the same substance.

The discussion of solidification microstructure above applies to pure substances and single-phase solid solutions (alloys). Although this book is concerned primarily with single-phase materials, it would now be beneficial to describe briefly the microstructures of a special type of multiphase alloy known as a *eutectic*. Eutectics are generally fine grained and uniformly dispersed. Like a pure single phase, a eutectic melts sharply at a constant temperature to form a liquid of the same composition. The simplest type of eutectic is the binary eutectic system containing no solid-phase miscibility and complete liquid phase (melt) miscibility between the two components (e.g., the Ag–Si system). On cooling, both components form nuclei and solidify simultaneously at the eutectic composition as two separate pure phases. This is termed *coupled growth* and it leads to a periodic concentration profile in the liquid close to the interface that decays in the direction perpendicular to the interface much faster than in single-phase solidification.

There are several methods for solidifying eutectics at conventional cooling rates, including the laser floating zone method, the edge-defined film-fed growth technique, the Bridgman method, and the micro-pulling down method. Generally, high volume fractions of both phases will tend to promote lamellar structures. If one phase is present in a small volume fraction, that phase tends to solidify as fibers. However, some eutectic growths show no regularity in the distribution of the phases. Eutectic microstructures normally exhibit small interphase spacing and the phases tend to grow with distinctly shaped particles of one phase in a matrix of the other phase. The microstructure will be affected by the cooling rate; it is possible for a eutectic alloy to contain some dendritic morphology, especially if it is cooled relatively rapidly. The microstructures of *hypo-* or *hypereutectic* compositions normally consist of large particles of the primary phase (the component that begins to freeze first) surrounded by fine eutectic structure. Often, the primary particles will show a dendritic origin, but they can transform into *idiomorphic grains* (having their own characteristic shape), reflecting the phase's crystal structure (Baker, 1992).

Photo courtesy of Dr. Pawel Tomaszewski, Institute of Low Temperature and Structure Research, Polish Academy of Sciences. Reproduced with permission.

Jan Czochralski (1885–1953) moved from his homeland of Poland to Germany in 1904 and received the chemist-engineer degree in 1910 from the Charlottenburg Polytechnic in Berlin, having worked in various positions at pharmacies and laboratories while attending school. His interests were in physical metallurgy, especially solidification, crystallization, corrosion, and plastic deformation. During his professional career, Czochralski published nearly 100 papers. The first, published in 1913 with his supervisor, Wichard von Moellendorff at the Allgemeinen Elecrizitaets-Gesellschaft (The General Electricity Company), was concerned with the movements of atoms during plastic deformation of single crystals, noteworthy in preceding the edge dislocation theory of Orowan, Taylor, and Polanyi by 20 years. In 1916, Czochralski serendipitously discovered a monocrystalline growth

method when he accidentally dipped his pen into a crucible of molten tin rather than his inkwell. He immediately pulled his pen out to discover that a thin thread of solidified metal was hanging from the nib. He replaced the nib with a capillary and verified that the crystallized metal was a single crystal. This method was to eventually pave the way for the processing of modern semiconductors after Bell Labs used the technique in 1950 to produce single crystals of germanium. Czochralski turned down an offer by Henry Ford to work in the United States, instead accepting a proposal by the Polish president in 1929 to return to Poland from Germany, where he had resided for 24 years. After receiving an honorary doctorate that same year from Warsaw University of Technology, Czochralski became a professor in the department of chemistry in 1930, eventually forming the laboratory, and later institute, of metallurgy and metals science. However, he was stripped of his professorship in 1945, due to accusations that he collaborated with the German occupation forces during World War II. Czochralski was later cleared of any wrongdoing, but he spent the remainder of his days running a small private firm that produced cosmetics and household chemicals.

Source: Professor Czochralski — Distinguished Scientist and Inventor, by K. J. Kurzydlowski and S. Mankowski; Jan Czochralski — Achievements, by Anna Pajaczkowska; and Professor Jan Czochralski (1885–1953) and His Contribution to the Art and Science of Crystal Growth, by Pawel Tomaszewski; *J. Am. Assoc. Crystal Growth*, **1998**, *2* (2), 12–18.

Metal–metal eutectics have been studied for many years due to their excellent mechanical properties. Recently, oxide–oxide eutectics were identified as materials with potential use in photonic crystals. For example, rodlike micrometer-scaled microstructures of terbium–scandium–aluminum garnet : terbium–scandium perovskite eutectics have been solidified by the micro-pulling-down method (Pawlak et al., 2006). If the phases are etched away, a pseudohexagonally packed dielectric periodic array of pillars or periodic array of pseudohexagonally packed holes in the dielectric material is left.

1.5.2. Molecular Self-Assembly in Materials Synthesis

The term *self-assembly* refers to the spontaneous formation (without human intervention) of ordered aggregates in systems at equilibrium or far from equilibrium. The driving force for a self-assembly process need not be chemical. For example, galaxies self-assemble via gravitational attractions. The physicochemical rules governing self-assembly are, of course, similar over various system length scales, although not necessarily identical. Here we consider only chemical forces. Chemical (molecular) self-assembly, henceforth referred to merely as self-assembly, is observed in nature over a wide range of length scales itself. Nevertheless, nanostructures are the most explored; self-assembly of micrometer-to-millimeter-sized and larger components from molecular-sized building blocks is a relatively

new area of materials research, as is the self-assembly of nonmolecular inorganic solids. The application of self-assembly in materials science and engineering, recently coined *mesoscale self-assembly* by Harvard University chemistry professor George Whitesides (Boncheva and Whitesides, 2005), also encompasses the fabrication of *mesocrystals* from nanoparticles that are, themselves, usually prepared by template-directed self-assembly. At the present time, the self-assembly of nonmolecular inorganic solids is mostly limited in application to monatonic substances and binary compounds (e.g., oxides, nitrides, sulfides), although some progress is being made in higher-order systems.

Self-assembly is essentially chemical fabrication. Like macroscale fabrication techniques, self-assembly allows a great deal of design flexibility in that it affords the opportunity to prepare materials with custom shapes or morphologies. The advantages of self-assembly include an increased level of architecture control and access to types of functionality unobtainable by most other types of liquid-phase techniques. For example, it has been demonstrated that materials with nonlinear optical properties (e.g., second harmonic generation), which require noncentrosymmetric structures, can be self-assembled from achiral molecules.

Control of lattice architecture and/or morphology may be attained in self-assembly by geometrical constraints of the building blocks, or by restriction of the space in which the assembly occurs. The latter approach is a type of *templating*. For the most part, advantage has been taken of this approach toward the synthesis of nanostructures. Various types of agents possessing the desired shape and size may act as templates, with a function similar in principle to that of molds used in industrial casting techniques. The pores of membranes produced by the sol–gel technique (Section 4.3), for example, have been used as templates for the synthesis of semiconductor oxide micro- and nanostructures. Ionic liquids (ILs), a class of reaction media with self-organized solvent structures (Section 4.4), have also been used in the synthesis of self-assembled, highly organized nanostructures with exceptional quality. The capability of self-assembly for facilitating obtainment of unique architectures is perhaps best exemplified by the low-surface-area hollow porous spheres comprised of interconnected hexagonal noble metal (e.g., Ag, Au) rings, which have been prepared on drops of liquid. The hexagonal rings were first fabricated by a multistep process involving photolithography and electrodeposition. Self-assembly of the rings into a sphere was then driven by capillary forces of attraction, while subsequent electroplating of silver on the rings welded them together (Huck et al., 1998).

It is instructive to compare these porous spheres (i.e., where all the edges of each hexagonal ring are adjoined to one other hexagonal ring to construct the sphere) with spherical particles prepared by alternative routes. Consider the nonhollow spherical conglomerations of nanoscale cobalt hexagonal flakes formed by hydrothermal reduction, in which the flakes are radially directed toward the center of the sphere. As with the noble metal spheres, the building blocks (flakes) must first be prepared. For the cobalt spheres, the nanoplatelets were chemically synthesized from surfactant-containing aqueous solutions of cobalt chloride. Assembly of the flakes into spheres via hydrothermal reduction is

thought to involve interfacial tension and the hydrophilic surfaces of the cobalt (Hou et al., 2005). Small hollow spheres of titanium dioxide have also been prepared by deposition on carbon spheres followed by calcination to remove the sacrificial carbon core (Zhang et al., 2006). Oxides of iron, nickel, cobalt, cerium, magnesium, and copper have been prepared as hollow spheres by a hydrothermal approach, but the spherical shells obtained are comprised of nanoparticles with high surface areas. The various spherical particles just discussed, all of which have potential technological uses (e.g., catalysis, drug-carrying and controlled release, magnetic recording, microcapsule reactors) are illustrated in Figure 1.9.

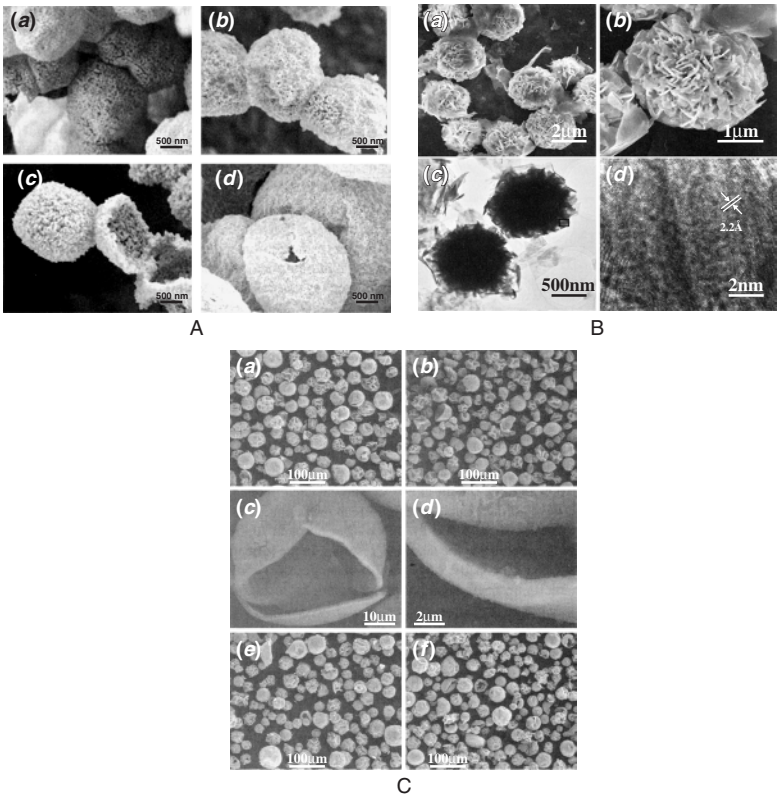

Figure 1.9 Various mesoscale spherical particles. Panel A: scanning electrom micrographs(GEMs) of (*a*) NiO, (*b*) Co_3O_4, (*c*) CeO_2, and (*d*) MgO hollow spheres. (Reprinted with permission from Titirici et al., 2006. Copyright © American Chemical Society.) Panel B: SEM images at (*a*) a survey, (*b*) higher resolution, transmission electrom micrographis and at (*c*) low resolution and (*d*) high resolution of Co spheres. (Reprinted with permission from Hou et al., 2005. Copyright © American Chemical Society.) Panel C: SEM images of hollow titania microparticles at (*a*) 400°C, (b–d) 400°C, (*e*) 600°C, and (*f*) 700°C. (Reprinted with permission from Zhang et al., 2006. Copyright © American Chemical Society.)

Control of lattice architecture may also be attained in self-assembly by a variety of other means. A frequently used method involves the use of structure-directing groups, also called *templating agents* (or again, just *templates* for short). Examples of *mesoscale* nonmolecular inorganic materials that have been synthesized by templated self-assembly include micrometers-long semiconducting CuS microtubes (assisted by acetic acid), $BaSO_4$ bundles (assisted by the sodium salt of polyacrylic acid), mesoporous silica with controlled pore sizes and shapes (aerosol-assisted), hollow titanium dioxide colloidal crystals (surface tension–assisted), and various silicon arrays.

In the simplest cases (e.g., constrained dimensionality), lattice architecture can be anticipated by considering both the molecular symmetries and the propagation of noncovalent interactions between structure-directing groups, which may be portions of the interacting molecules themselves (Ward, 2005). Consider the guanidinium carbocation $[C(NH_2)_3^+]$ and the sulfonate anion (RSO_3^-), each possessing threefold rotational symmetry (trigonal stereochemistry) about the central atom: ideally, $D_{3\boldsymbol{h}}$ and $C_{3\mathbf{v}}$ point group symmetries, respectively. Guanidinium organomonosulfonate salts (one sulfonate anion per organic group R) would be expected to self-assemble into a network of N–H···O–S hydrogen bonds that can be viewed as a sheet comprised of ribbons fused along their edges, suggesting the two-dimensional quasihexagonal motif illustrated in Figure 1.10*a*. Three-dimensional frameworks can be assembled from guanidinium organodisulfonate salts (two sulfonate groups attached to each organic group R), where the organic R groups then function as pillars supporting inclusion cavities between adjacent sheets. The constrained dimensionality thus enforces host–guest systems with lamellar architectures (Figure 1.10*b*), which crystallize in orthorhombic or monoclinic space groups. These systems are of interest for their potential use in optoelectronics, chemical separations, and confined chemical reactions.

The use of organic templating agents highlights the pivotal role of weak and noncovalent intermolecular forces in driving self-assembly. As indicated in the preceding paragraph, molecules, which are not necessarily components of the intended structure, may be used as templates for directing self-assembly. Such "guest" species are integral to promoting assembly of frameworks containing large open spaces, as with the guanidinium organodisulfonate salts, supplying the cohesive energy required for crystallization. Successful production of desired lattice architecture often hinges on the de novo design of these structure-directing agents themselves. The goal is to choose molecules with particular structural motifs conducive to the formation of the desired framework in the product. Unfortunately, the frameworks may collapse upon attempted removal of the template (e.g., by heating). This means that one may possibly be faced with the difficult task of phase-separating the templating agent from the desired product if removal of the template is necessary.

Despite these difficulties, mesoscale self-assembly of inorganic materials holds promise. In fact, it is believed that the importance of self-assembly in the manufacturing of electronics, photonics, optics, and robotics mesoscale components could conceivably supersede its importance in the molecular and nanoscale sciences. Some hybrid organic–inorganic systems have attracted attention because

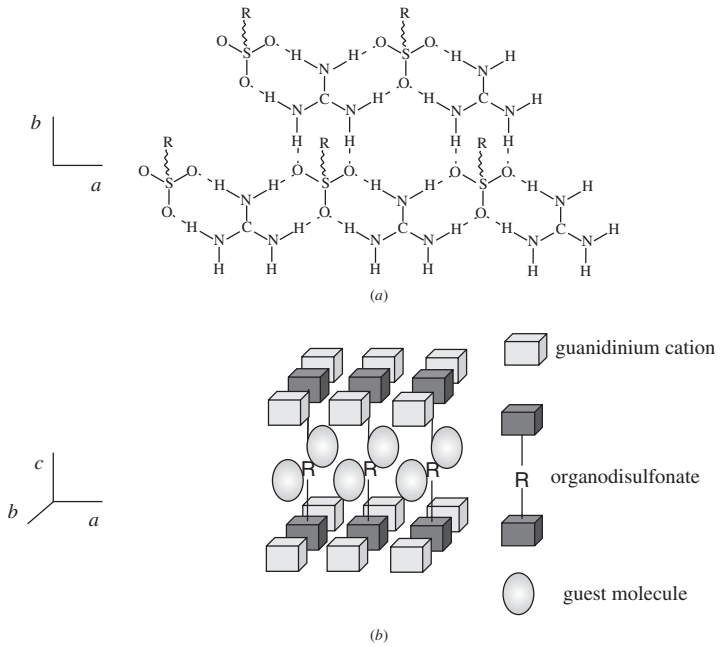

Figure 1.10 (*a*) Guanidinium organomonosulfonate salts (one sulfonate anion per organic group R) self-assembled into a quasihexagonal two-dimensional network of N–H···O-S hydrogen bonds. (From Russell et al., 1994.) (*b*) Three-dimensional lamellar frameworks assembled from guanidinium organodisulfonate salts (two sulfonate groups attached to each organic group R), where the organic R groups function as pillars supporting inclusion cavities capable of holding guest molecules between adjacent sheets.

of their novel properties. For example, organic–inorganic perovskites have unique magnetic, optical, thermochromic, and electrical properties and structural flexibility (Li et al., 2006). It has been shown that inorganic superlattices (composite heterostructures that may be described as periodic multilayers where the unit cell consists of chemically different successive layers) can also be templated by molecular assemblies. Moreover, it has been demonstrated that the structures of these superlattices can kinetically control some intralayer solid-state reactions. This is described a bit more in Section 2.5.3. There is also evidence suggesting that self-assembly is important at some point during the formation of the open-framework architectures of metal phosphates, templated by organic amines. Self-assembly is probably involved in the transformation of one-dimensional chains (containing vertex-shared four-membered rings) and ladder structures (containing edge-shared four-membered rings) into two-dimensional layer structures and three-dimensional channel-containing structures (Rao, 2001).

In contrast to mesoscale assemblies, mesocrystals are considered intermediates on the formation pathway to single crystals (Cölfen and Yu, 2005). The full growth mechanism has been reported for very few mesocrystals, two of

which are copper oxalate and calcite. Nanocrystals of copper oxalate have been found to arrange into mesocrystals that can be modified morphologically by the addition of face-selective hydroxymethylpropylcellulose. In other studies, crystallization of calcite ($CaCO_3$) from concentrated calcium chloride solutions by the CO_2 gas diffusion technique in the presence of polystyrene sulfonate (Wang et al., 2005), and by copolymer latex particles functionalized by surface carboxylate groups (Lu et al., 2005), is found to be capable of yielding crystals with irregular morphology. Morphology can be varied systematically from the typical calcite rhombohedra via rounded edges and truncated triangles to finally, concavely bended lenslike superstructures. The crystals are apparently well-faceted in light microscopy. However, electron microscopy analysis has confirmed that they are highly porous and composed of almost perfectly 3D-aligned calcite nanocrystals scaffolded to the final curved superstructures (i.e., that they are mesocrystals). At high supersaturation, superstructures with changed symmetry are found.

1.6. STRUCTURES OF GLASSY AND QUASICRYSTALLINE PHASES

In Chapter 4 we discuss the thermodynamic and kinetic aspects of rapidly solidifying certain types of liquid phases, whereupon glassy and quasicrystalline solids are obtained. Here, we describe those structures briefly. Glasses are monolithic amorphous materials, absent long-range structural order, as well as grain boundaries and other crystalline defects. The term *long-range order* (LRO) refers to regularity in the arrangement of the material's atomic or molecular constituents on a length scale a few times larger than the size of these groups. A glass also possesses *short-range order* (SRO) and *medium-range order* (MRO). Natural glasses form when certain types of rock melt as a result of volcanic activity, lightning strikes, or meteorite impacts, followed by very rapid cooling and solidification. Stone-age peoples are believed to have used some of these naturally formed amorphous materials as tools for cutting. An example is *fused quartz*, or *quartz glass*, formed by the melting and rapid cooling of pure silica. Upon rapid solidification, the short-range order (geometry) of the SiO_4 tetrahedra is preserved but not the long-range crystalline order of quartz. The structure of quartz involves corkscrewing (helical) chains of SiO_4. The corkscrew takes four tetrahedra, or three turns, to repeat, each tetrahedron essentially being rotated 120°. The chains are aligned along one axis of the crystal and interconnected to two other chains at each tetrahedron. The Si–O–Si bond angle between interconnected tetrahedra is nominally about 145° degrees. As in quartz, every oxygen atom in fused quartz is also bonded to two silicon atoms (each SiO_4 tetrahedron is connected to four other tetrahedra), but the tetrahedra are polymerized into a network of rings of different sizes, occurring in a wide range of geometries. Hence, in quartz glass there is a distribution of Si–O–Si bond and Si–O–Si–O torsion angles.

The very high temperatures required to melt quartz were not attainable by early craftspersons. Hence, they prepared sodium silicate glass by mixing together and

melting sodium carbonate with sand. The structure of this *water glass* is similar to that of quartz glass except that with the random insertion of sodium ions within the network, nonbridging oxygen atoms (i.e., oxygen atoms bonded to a single silicon atom) are produced. The first glassy phase prepared in this manner was either in Egypt or Mesopotamia in the form of ceramic glazes. Around the middle of the second millennium B.C., glassware was being made, principally in the form of pots and vases. The first glassmaking manual, dating back to 650 B.C., appears to have come from Assyria. The next major breakthrough in the evolution of the art was glassblowing, which originated sometime around A.D.1 in the Sidon–Babylonian region. Glassmaking continued to evolve throughout Europe, with many key advances necessary for mass production made in the latter stages of the Industrial Revolution. We have much more to say about the glass formation process in Chapter 4.

A fairly recent event that attracted much attention within the crystallographic community was the discovery of metastable quasicrystals of an Al–Mn alloy with fivefold rotational symmetry in the 1980s at the U.S. National Bureau of Standards (now the National Institute for Standards and Technology) by Shechtman et al. (1984). Crystals are three-dimensional and therefore are limited to having only have one-, two-, three-, four-, or sixfold rotation axes; all other rotational symmetries are forbidden. Unlike crystals, which may or may not display rotational order, quasicrystals possess *only* rotational order and no three-dimensional translational periodicity. However, the long-range structure is coherent enough to scatter incoming waves so as to produce an interference pattern. Hence, the quasicrystalline state is manifested by the occurrence of sharp diffraction spots, indicative of long-range order, but with the presence of a noncrystallographic rotational symmetry.

Aperiodic plane-filling (two-dimensional) patterns, based on various basis sets of tiles, have actually been studied for some time. In fact, it is believed that Islamic architects and mathematicians created the first such patterns over 500 years ago (Lu and Steinhardt, 2007). In his 1964 mathematics doctoral thesis at Harvard, Robert Berger developed a set of 20,426 essentially square tiles called *Wang dominos* (squares with different colored edges or geometrically altered to prevent periodic arrangements) that tiled nonperiodically. (He later reduced this to a set of 104.) Stanford University professor Donald Knuth (b. 1938) found a set of 92 in 1968. In 1971, Raphael Robinson (1911–1995), professor of mathematics at the University of California–Berkeley, devised a set of six non-Wang aperiodic tiles. In 1973, the Oxford mathematician Roger Penrose (b. 1931) discovered a nonperiodic tiling in two dimensions with pentagonal symmetry by combining a set of six tiles (Figure 1.11). He subsequently reduced this to a set of four "kite" and "dart" tiles (altered so that they form an aperiodic set) and finally, a tiling based on a set of two rhombuses (Penrose, 1974). Each rhombus is a symmetrical tile, made by the combination of the two triangles found in the geometry of the pentagon. Kites and darts may be obtained from rhombuses, and vice versa. Penrose tilings may be considered two-dimensional quasicrystals.

Since the initial discovery of metastable quasicrystals, many ternary intermetallic compounds have been produced in the quasicrystalline state, which are thermodynamically stable at room temperature. These have been obtained

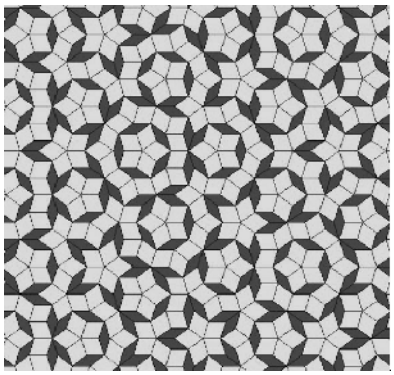

Figure 1.11 Portion of a Penrose tiling based on two rhombuses. Penrose tilings are nonperiodic tilings of the plane and are two-dimensional analogs of quasicrystals. (Diagram created by the free Windows application "Bob's Rhombus Walker," v. 3.0.19, JKS Software, Stamford, CT.)

primarily by solidifying phases with equilibrium crystal structures containing icosahedrally packed groups of atoms (i.e., phases containing icosahedral point group symmetry) at conventional cooling rates. The quasicrystalline phases form at compositions close to the related crystalline phases. We discuss quasicrystalline formation in Chapter 4. For now, we restrict the discussion to the structural aspects of these phases.

The icosahedron is one of the five Platonic solids, or regular polyhedra. A regular polygon is one with equivalent vertices, equivalent edges, and equivalent faces. The icosahedron has 20 faces, 12 vertices, 30 edges, and six fivefold proper rotation axes (collinear with six tenfold improper rotation axes). Icosahedral coordination ($Z = 12$) and other coordination polytetrahedra with coordination numbers $Z = 14$, 15, and 16 are a major component of some liquid structures, more stable than a close-packed structure, as demonstrated by F. C. Frank and J. Kasper (Frank and Kasper, 1958a, b). When these liquid structures are solidified, the resulting structure has icosahedra threaded by a network of wedge disclinations, having resisted reconstruction into crystalline units with 3D translational periodicity (Mackay and kramer, 1985; Turnbull and Aziz, 2000). Stable ternary intermetallic icosahedral quasicrystals are known from the systems Al–Li–Cu, Al–Pd–Mn, and Zn–Mg–Ln. Several other ternary systems yield metastable icosahedral quasicrystals (Lalena and Cleary, 2005).

Some stable ternary intermetallic phases have been found that are quasiperiodic in two dimensions and periodic in the third. These are from the systems Al–Ni–Co, Al–Cu–Co, and Al–Mn–Pd. They contain decagonally packed groups of atoms (local tenfold rotational symmetry). It should be noted that there are also known metastable quasicrystals with local eightfold rotational symmetry (octagonal) and 12-fold rotational symmetry (dodecagonal) as well. The dodecahedron is also one of the five Platonic solids (Lalena and Cleary, 2005).

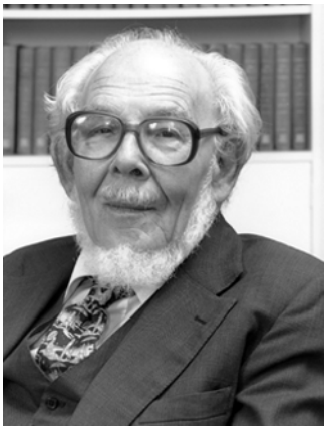

Photo courtesy of the Royal Society. Copyright © The Royal Society. Reproduced with permission.

Sir Frederick Charles Frank (1911–1998) received his Ph.D. in 1937 from Oxford University, followed by a postdoctoral position at the Kaiser Wilhelm Institut für Physik in Berlin. During World War II, Frank was involved with the British Chemical Defense Research Establishment, and because of his keen powers of observation and interpretation, he was later transferred to Scientific Intelligence at the British Air Ministry. In 1946, Frank joined the H. H. Wills Physics Laboratory at the University of Bristol under its director, Nevill Mott, who encouraged him to look into problems concerned with crystal growth and the plastic deformation of metallic crystals. A stream of successes followed, establishing his scientific fame, as evidenced by many eponyms: the Frank–Read source, the Frank dislocation, Frank's rule, Frank–Kasper phases. His theoretical work has been the foundation of research by innumerable scientists from around the world. Frank was awarded the Order of the British Empire (OBE) Medal in 1946, elected a Fellow of the Royal Society (FRS) in 1954, and was knighted in 1977.

Source: Obituary of Sir Charles Frank OBE FRS, 1911–1998, prepared by A. R. Lang for the British Crystallographic Association. Copyright © 1998.

For a periodic space-filling lattice, one can translate the pattern by a certain distance in a certain direction, and every point in the translated portion will coincide with a point in the original lattice. However, with a space-filling quasilattice, this operation is not possible. One can take a bounded region and translate it to coincide exactly with some other part of the original pattern. Such a representative portion constitutes a kind of "unit cell" of the quasilattice. There are two different complementary packable rhombohedra, an acute-angled and an obtuse-angled rhombohedra that can be combined in a space-filling manner to form rhombic dodecahedra, icosahedra, triacontahedra, and ultimately, quasicrystals (Lalena, 2006).

A relationship actually exists between periodic and quasiperiodic patterns such that any quasilattice may be formed from a periodic lattice in some higher dimension (Cahn, 2001). The points that are projected to the "physical" three-dimensional space are usually selected by cutting out a "slice" from the higher-dimensional lattice. Therefore, this method of constructing a quasiperiodic lattice is known as the *cut-and-project method*. In fact, the pattern for *any* three-dimensional quasilattice (e.g., icosahedral symmetry) can be obtained by a suitable projection of points from some six-dimensional periodic space lattice into a three-dimensional subspace. The idea is to project part of the lattice points of the higher-dimensional lattice to three-dimensional space, choosing the projection such that one preserves the rotational symmetry. The set of points so obtained are called a *Meyer set* after French mathematician Yves Meyer (b. 1939), who first studied cut-and-project sets systematically in harmonic analysis (Lalena, 2006).

Without relying on the cut-and-project technique, Rabson et al. (1991) have computed all the three-dimensional quasicrystallographic space groups with n-fold axial point groups and standard lattices by a method that treats crystals and quasicrystals in equivalent fashion, taking advantage of the more readily apparent symmetry in reciprocal space than in direct space. The familiar three-dimensional crystallographic space groups with axial point groups emerge simply and directly as special cases of the general n-fold three-dimensional quasicrystallographic treatment with $n = 3$, 4, and 6. Additionally, they have given a general discussion of extinctions in quasicrystals as well as a simple three-dimensional geometrical specification of the extinctions for each axial space group.

The central issue in quasicrystal structure analysis, however, has been the locations of the atoms. Unlike with the structure determination of crystals, for quasicrystals it has proven rather difficult to acquire a conclusive solution based on the diffraction intensities. This is due to the fact that several quasiperiodic structural models, differing in local atomic arrangements, can generate very similar intensity distributions (with crystals, these are known as *homometric structures*). Consequently, direct observation, such as from high-resolution electron microscopy, is essentially required for solving quasicrystalline atomic structure. As recently discussed (Lalena, 2006), the International Union of Crystallography (IUCr) was inspired by the growing numbers of quasicrystals and the success of Fourier space crystallography in explaining quasiperiodic and periodic crystals alike. In 1991, the IUCr shifted the essential attribute of crystallinity from direct space to reciprocal space by redefining the term *crystal* to mean "any solid having an essentially discrete diffraction diagram" (Lifshitz and Mermin, 1992; Lifshitz, 1995).

REFERENCES

Baker, H., Ed. *ASM Handbook*, Vol. *3*, Alloy Phase Diagrams, ASM International, Materials Park, OH, **1992**.

Barlow, W. Z. *Krystallogr. Mineral*. **1894**, *23*, 1–63.

Bhadeshia, H. K. D. H. *Worked Examples in the Geometry of Crystals*, Institute of Metals, London, **1987**.

Bollman, W. *Philos. Mag. A.* **1967**, *6*, 363.

Bollman, W. *Crystal Defects and Crystallian Interfaces*, Springer Verlag, Berlin, **1970**.

Boncheva, M.; Whitesides, G. M. *Mater. Res. Soc. Bull*. **2005**, *30*(10), 736–742.

Brandon, D. G.; Ralph, B.; Ranganathan, S.; Wald, M. S. *Acta Metall*. **1964**, *12*, 813.

Bravais, A. J. *Ecole Polytech*. **1850**, *19*, 1–128.

Bravais, A. *Études Cristallographiques*, Gauthier-Villars, Paris, **1866**.

Bridgman, P. W. *Proc. Am. Acad. Arts Sci*. **1926**, *60*, 306.

Buerger, J. M. *Am. Mineral*. **1945**, *30*, 469–482.

Buerger, J. M. *Elementary Crystallography*, MIT Press, Cambridge, MA, **1978**.

Burton, W. K.; Cabrera, N.; Frank, F. C. *Philos. Trans. R. Soc. London A*. **1951**, *243*, 299.

Cahn, J. W. *J. Res. Nat. Inst. Stand. Technol*. **2001**, *106*, 975–982.

Chen, F.-R.; King, A. H. *Acta Crystallogr. B* **1988**, *43*, 416.

Cölfen, H.; Yu, S.-H. *Mater. Res. Soc. Bull*. **2005**, *30*(10), 727–735.

Czochralski, J. Z. *Phys. Chem*. **1918**, *92*, 219–221.

Donnay, J. D. H.; Harker, D. *Am. Mineral*. **1937**, *22*, 446.

Dowty, E. *Am. Mineral*. **1976**, *61*, 448.

Fedorov, E. S. *Proc. Imp. Saint Petersburg Soc. Ser*. **1891**, *2*(28), 345–389 (in Russian).

Fedorov, E. S. *Proc. Imp. Saint Petersburg Soc. Ser*. **1891a**, *2*(28) 1–146 (in Russian).

Frank, F. C.; Kasper, J. S. *Acta Crystallogr*. **1958a**, *11*, 184.

Frank, F. C.; Kasper, J. S. *Acta Crystallogr*. **1958b**, *12*, 483.

Friedel, G. *Bull. Soc. Fr. Mineral*. **1907**, *30*, 326.

Hannon, J. B.; Shenoy, V. B.; Schwarz, K. W. *Science*. **2006**, *313*, 1266.

Hartman, P.; Perdok, W. G. *Acta Crystallogr*. **1955a**, *8*, 49–52.

Hartman, P.; Perdok, W. G. *Acta Crystallogr*. **1955b**, *8*, 521–524.

Hartman, P.; Perdok, W. G. *Acta Crystallogr*. **1955c**, *8*, 525–529.

Hermann, C. Z. *Kristallogr*. **1928**, *68*, 257.

Hermann, C. Z. *Kristallogr*. **1931**, *76*, 559.

Hou, Y.; Kondoh, H.; Ohta, T. *Chem. Mater*. **2005**, *17*, 3994.

Hessel, J. F. C. Jr. *Gehler's Physikalische Wöterbuch*, Schwikert, Leipzig, Germany, **1830**, pp. 1023–1360. Reprinted in *Ostwald's Klassiker der Exakten Wissenschaften*, Engelmann, Leipzig, Germany, 1897.

Huck, W. T. S.; Trin, J.; Whitesides, G. M. *J. Am. Chen. Soc*. **1998**, *120*, 8267.

Kannan, C. V.; Ganesamoorthy, S.; Kumaragurubaran, S.; Subramanian, C.; Sundar, R.; Ramasamy, P. *Cryst. Res. Technol*. **2002**, *37*(10), 1049–1057.

Kossel, W. *Nachr. Ges. Wiss. Goettingen*. **1927**, 135.

Lalena, J. N. *Crystallogr. Rev*. **2006**, *12*, 125.

Lalena, J. N.; Cleary, D. A. *Principles of Inorganic Materials Design*, Wiley, Hoboken, NJ, **2005**.

Li, Y. Y.; Lin, C. K.; Zheng, G. L.; Cheng, Z. Y.; You, H.; Wang, W. D.; Lin, J. *Chem. Mater*. **2006**, *18*, 3463.

Lifshitz, R. In *Lecture Notes for the International School on Quasicrystals*, Balatonfüred, Hungary, May 13–20, **1995**.

Lifshitz, R.; Mermin, N. D. *Acta Crystallogr. A*. **1992**, *48*, 928.

Lin, C. T.; Liang, B.; Chen, H. C. *J. Cryst. Growth*. **2002**, 237–239, 778–782.

Lin, S.-K. *J. Chem. Inf. Comput. Sci*. **1996**, *36*, 367–376.

Lin, S.-K. *Int. J. Mol. Sci*. **2001**, *2*, 10–39.

Lu, C.; Qi, L.; Cong, H.; Wang, X.; Yang, J.; Yang, L.; Zhang, D.; Ma, J.; Cao, W. *Chem. Mater*. **2005**, *17*, 5218–5224.

Lu, P. J.; Steinhardt, P. J. *Science*. **2007**, *315*(5815), 1106.

Mackay, A. L.; Kramer, P. *Nature*. **1985**, *316*, 17.

Mauguin, C. Z. *Kristallogr*. **1931**, *76*, 542.

Neumann, F. E. *Pogendorff Ann. Phys*. **1833**, *27*, 240.

Nye, J. F. *Physical Properties of Crystals: Their Representation by Tensors and Matrices*, Oxford University Press, London, **1957**.

Pawlak, D. A.; Kolodziejak, K.; Turczynski, S.; Kisielewski., J.; Rozniatowski, K.; Diduszko, R.; Kaczkan, M.; Malinowski, M. *Chem. Mater*. **2006**, *18*, 2450–2457.

Penrose, R. *Bull. Inst. Math. Appl*. **1974**, *10*, 266–271.

Rabson, D. A.; Mermin, N. D.; Rokhsar, D. S.; Wright, D. C. *Rev. Mod. Phys*. **1991**, *63*, 699–733.

Rao, C. N. R. *Proc. Indian Acad. Sci*. (*Chem. Soc*.). **2001**, *113*, 363–374.

Rosen, J. *Symmetry in Science: An Introduction to the General Theory*, Springer-Verlag, New York, **1996**.

Runyan, W. R.; Bean, K. E. *Semiconductor Integrated Circuit Processing Technology*, Addison-Wesley, Reading, MA, **1990**.

Russell, V. A.; Etter, M. C.; Ward, M. D. J. *Am. Chem. Soc*. **1994**, *116*, 1941.

Schönflies, A. M. *Kristallsysteme und Kristallstruktur*, Teubner, Leipzig, Germany, **1891**.

Shechtman, D.; Blech, L.; Gratias, D.; Cahn, J. W. *Phys. Rev. Lett*. **1984**, *53*, 1951.

Shewmon, P. *Diffusion in Solids*, Minerals, Metals, and Materials Society, Warrendale, PA, **1989**.

Stockbarger, D. C. *Rev. Sci. Instrum*. **1936**, *7*, 133.

Stranski, I. N. *Z. Phys. Chem*. **1928** *136*, 259.

Titirici, M.-M.; Antonietti, M.; Thomas, A. *Chem Mater*. **2006**, *18*, 3808.

Wang, T.; Cölfen, H.; Antonietti, M. J. *Am. Chem. Soc*. **2005**, *127*(10), 3246–3247.

Ward, M. D. *Mater. Res. Soc. Bull*. **2005**, *30*(10), 705–712.

Watanabe, T. *Res. Mech*. **1984**, *11*, 47.

Watanabe, T. In *Grain Boundary Engineering*, U., Erb, and G., Palumbo, Eds., CIM, Montreal, Canada, **1993**.

Wolfe, D.; Lutsko, J. F. *Z. Kristall*. **1989**, *189*, 239.

Zhang, D.; Yang, D.; Zhang, H.; Lu, C.; Qi, L. *Chem. Mater*. **2006**, *18*, 3477.